

October 2018

Automated Optical Inspection of MEMS Based Cochlear Implant Hydrophones

Angela MacLeod

Worcester Polytechnic Institute

Colette Elaine Ruden

Worcester Polytechnic Institute

Libertad Escobar

Worcester Polytechnic Institute

Sarah Elizabeth Bachli

Worcester Polytechnic Institute

Follow this and additional works at: <https://digitalcommons.wpi.edu/mqp-all>

Repository Citation

MacLeod, A., Ruden, C. E., Escobar, L., & Bachli, S. E. (2018). *Automated Optical Inspection of MEMS Based Cochlear Implant Hydrophones*. Retrieved from <https://digitalcommons.wpi.edu/mqp-all/6607>

This Unrestricted is brought to you for free and open access by the Major Qualifying Projects at Digital WPI. It has been accepted for inclusion in Major Qualifying Projects (All Years) by an authorized administrator of Digital WPI. For more information, please contact digitalwpi@wpi.edu.

Automated Optical Inspection of MEMS Based Cochlear Implant Hydrophones

A Major Qualifying Project
Submitted to the Faculty of
Worcester Polytechnic Institute
in partial fulfillment of the requirements for the
Degree in Bachelor of Science
in
Mechanical Engineering

By

Sarah Bachli

Libertad Escobar

Angela MacLeod

Colette Ruden

Date: October 29, 2018

Sponsoring Organization: UniversitätsSpital Zurich

Project Advisor: Professor Sarah Jane Wodin-Schwartz

This report represents work of WPI undergraduate students submitted to the faculty as evidence of a degree requirement. WPI routinely publishes these reports on its web site without editorial or peer review. For more information about the projects program at WPI, see <http://www.wpi.edu/Academics/Projects>.



**UniversitätsSpital
Zürich**

Table of Contents

Table of Contents	i
List of Figures	iii
List of Tables	v
Acknowledgments.....	1
Abstract	2
Chapter 1: Introduction	3
Chapter 2: Background	4
2.1 Cochlear Implants	4
2.2 Current State of Research at USZ.....	4
2.3 Optical Inspection Overview	7
Automation of a Microscope for Optical Inspection	7
Automation of Membrane Optical Inspection	7
Chapter 3: Methodology	9
3.1 Design and Implementation of Hardware	9
3.1.1 Z-Axis Control System	10
3.1.2 X and Y Axis Control System	15
3.2 Design of Image Capture and Image Processing Scripts	20
3.2.1 Image Capture Script	20
3.2.2 Image Processing Script.....	21
3.3 Verification and Optimization of Control System	23
3.3.1 Investigation of Potential Physical Error	24
3.3.2 Establishment of Control System Characteristics.....	26
3.3.3 Optimization of System Functionality	31
3.4 Summary of Methodology	36
Chapter 4: Results and Discussion.....	37
4.1 Potential Error Investigation Results	37
4.2 Control System Characterization	39
4.2.1 Magnification Level Investigation	39
4.2.2 Pixel Size Calculations	39
4.2.3 Z-Axis Dial Calibration	40
4.2.4 X and Y Axis Preliminary Dial Calibration.....	43
4.2.5 Measurement Parameters	44
4.3 Optimization Testing Results.....	47

4.3.1 Design of Experiments for Image Capture Presets	47
4.3.2 Convergence Testing for Slice Resolution of Image Capture	49
4.3.4 Convergence Testing for Cell Radius and Cell Pitch of Image Processing.....	51
Chapter 5: Conclusion.....	55
Chapter 6: Recommendations	57
6.1 Z-Axis Recommendations	57
6.2 X & Y Axis Recommendations	58
References.....	59
Appendix A: Interview with Dr. Lukas Prochazka for current manual process.....	61
Appendix B: Wiring of Z-Axis Control System.....	62
Appendix C: Wiring of X and Y Axis Control System	64
Appendix D: Stage Offset Testing.....	65
Appendix E: Focusing Dial Calibration and 5x vs. 10x data results	66
Appendix F: Design of Experiment Analysis for Image Capture Presets	69
Appendix G: Convergence Testing for Slice Resolution measuring diameter	71
Appendix H: Convergence Testing Data Analysis	72
Appendix I: User Manual for the Automated Leica Microscope Optical Inspection System	75

List of Figures

Figure 1: Intracochlear Acoustics Receiver (ICAR) UniversitätsSpital Zurich, (n.d.a).....	5
Figure 2: ICAR Titanium Layers UniversitätsSpital Zurich, (n.d.b).....	5
Figure 3: Control System Overview	9
Figure 4: Leica Light Microscope.....	10
Figure 5: Control System Overview	11
Figure 6: Z-Axis Control System Proof of Concept Model.....	12
Figure 7: Z-Axis Control System Prototype I.....	13
Figure 8: Z-Axis Dial Adapter CAD Model.....	13
Figure 9: Z-Axis Dial Adapter Final Design CAD Model	14
Figure 10: Z-Axis Dial Adapter Final Design	14
Figure 11: Distance between membranes in a sample holder.....	15
Figure 12: X and Y Axis Control System.....	15
Figure 13: X and Y Axis Dials on Leica Light Microscope	16
Figure 14: X and Y Axis Stepper Motor (Schrittmotor, n.d.).....	17
Figure 15: Design I - Stepper Motor to Microscope Stage Clamp	17
Figure 16: Design II - Preliminary X and Y Axis Dial Adapter Design with Hose Clamp Implementation (Cade, n.d.)	18
Figure 17: Design III - Motor Housing CAD Models (left and middle) and 3D Printed Models (right)	18
Figure 18: Design III - CAD Models of the X and Y Axis Dial Adapters (left and middle) and Final Dial Adapters (right).....	19
Figure 19: Design III - Motor Housing and Dial Adapters for X and Y	19
Figure 20: Slice Resolution Visual Definition.....	20
Figure 21: Overview of Image Capture Procedure	20
Figure 22: Cell Radius and Cell Pitch Example (figure not to scale).....	22
Figure 23: Overview of Image Processing Procedure	22
Figure 24: Stage Offset Testing Procedure (left), Stage Measurement Setup (middle) and Mahr Millimess Micrometer (right)	25
Figure 25: A 1 μm slice resolution unit equals 5 motor steps	25
Figure 26: Z-Axis Coarse and Fine Focusing Dials of Leica Light Microscope.....	27
Figure 27: Top (left) and Middle (right) Titanium Layers	27
Figure 28: Graphical Representation of Titanium Layer Thickness Verification Procedure	29
Figure 29: 2D Plot of Membrane Curvature with Data Cursors.....	30
Figure 30: Membrane Cross Sectional Area Tests	30
Figure 31: Membrane Naming Convention in Sample Holder.....	34
Figure 32: Effects of Cell Radius on 2D Plots.....	35
Figure 33: Effects of Cell Pitch on 2D Plots.....	35
Figure 34: Average Stage Offset per Slice Resolution	38

Figure 35: Membrane Sample at 5x, 10x, and 20x Magnification (left to right).....	39
Figure 36: Calibration Ruler Measurements of Width (left) and Height (right), each tick is 10 μm	40
Figure 37: Configuration Tested for Preliminary X and Y Axis Control Investigation	43
Figure 38: No Rotation - Membrane 1a.....	44
Figure 39: 10° Rotation - Membrane 1a	45
Figure 40: 90° Rotation - Membrane 1a	45
Figure 41: Membrane 14a.....	46
Figure 42: Example Pareto Chart of the Standardized Effects	47
Figure 43: Main Effects Plot of Frequency, Duration and Pause	48
Figure 44: Interaction Plot of Frequency, Duration, and Pause.....	48
Figure 45: Height Convergence for Slice Resolution	50
Figure 46: Effects of Cell Radius on 2D Plots.....	51
Figure 47: Effects of Cell Pitch on 2D Plots.....	51
Figure 48: Height Convergence for Cell Pitch of 25 pixels.....	52
Figure 49: Height Convergence Plot with a Cell Radius of 30 pixels (Test 2)	53
Figure 50: Height Convergence Plot with a Cell Radius of 20 pixels (Test 3)	53
Figure 51: Characterization of Hydrophone Sensor Membrane from August 14 th	55
Figure 52: Characterization of Hydrophone Sensor Membrane from October 5 th	56

List of Tables

Table 1: Overview of Image Capture Procedure	21
Table 2: Overview of Image Processing Procedure.....	23
Table 3: Distance to Travel per Direction for each Slice Resolution	25
Table 4: Titanium Layer Thickness Verification Procedure.....	28
Table 5: Corresponding Motor Steps to Slice Resolution	31
Table 6: Frequency and Duration Configurations	32
Table 7: DOE for Frequency/Duration and Pause Configurations	33
Table 8: Membrane Shape Configuration.....	34
Table 9: Average Stage Offset and Micrometer Tolerance Added.....	38
Table 10: Average Distance per Focusing Dial Increment.....	40
Table 11: Measured Titanium Layer Thickness	42
Table 12: Height and Diameter Measurements	46
Table 13: Configuration for Frequency/Duration and Pauses	49
Table 14: Convergence Data Summary for Slice Resolution	50
Table 15: Summary of Optimal Cell Radius and Cell Pitch Configurations	54

Acknowledgments

Our team would like to express our gratitude to the sponsor of this project, Dr. Ivo Dobrev from the UniversitätsSpital Zürich (USZ), for his dedicated support and commitment to the success of this project. Additionally, we would like to thank Dr. Lukas Prochazka and the ICAR research team at USZ for their assistance and for allowing us to share their workspace. Finally, thank you to our advisor from Worcester Polytechnic Institute, Professor Sarah Wodin-Schwartz for her guidance and insight provided over the course of the project.

Abstract

The goal of this project was to design and integrate an efficient automated optical inspection procedure to characterize hydrophone sensor membranes for the fully implantable cochlear implant in development at the UniversitätsSpital Zurich. These membranes are a vital component of the sensor for registering sound. This goal was accomplished through the research, design, and prototyping of control systems and programs for image capture and post-processing. The finalized procedure is time-saving and optimized for optical inspection tests which were previously not feasible. This project lays the foundation for the fully automated optical inspection of multiple hydrophone membranes. This allows researchers to draw conclusions from data comparison to produce functional fully implantable cochlear implants.

Chapter 1: Introduction

UniversitätsSpital Zurich (USZ) is leading research to develop an improved sensor component for the intracochlear acoustic receiver (ICAR) (Pfiffner et al, 2017). The USZ team is studying how the natural environment of the cochlea affects the sensitivity of the hydrophone component, which includes biocompatible membranes. The membrane post-manufacturing quality control process is made up of three main tests: quasi-static loading, acoustic loading, and optical inspection. The optical inspection of the membrane is manual, entails a large time commitment, and does not have set measurement parameters to compare sample-to-sample data (I. Dobrev, personal communication, August 14, 2018). This project focuses on automating the optical inspection and data collection process while developing a standard operating procedure for analysis and characterization of the membrane shape.

Chapter 2: Background

USZ is committed to developing active middle ear implants due to the expanding market and normalization of cochlear implant surgery. Within this environment of innovation, it is vital for researchers to visualize the effects of human and non-human surroundings on the micro-scale control systems of the implant.

2.1 Cochlear Implants

Cochlear implants are designed for individuals facing extensive hearing loss that cannot be corrected by standard hearing aids. This condition results from the absence of hair cells within the cochlea which convert changes in pressure to electrical impulses. Without the cells, these impulses cannot be registered by neurons and thus cannot be interpreted by the brain as sound.

Cochlear implants are essential for combating severe hearing loss because they mimic the function of the vital hair cells. The device's electrodes are inserted into the cochlea to receive vibrations from a microelectrical mechanical systems (MEMS) microphone and produce impulses that can be registered by the brain as sound (Yip et al, 2015).

Most commercially available cochlear implants contain an internal and external component. The internal ear component consists of the electrode array, circuitry to support the implant, a communication link to the exterior component, and a magnet. The external component consists of a microphone, battery, sound processor, transmitter, and a corresponding magnet (NIDCD, 2017). The external portion of the device is constantly exposed to damaging environmental conditions and may attract unwanted attention. Currently, cochlear implants are too large for all of the components to fit inside the ear. MEMS technology has the potential to rectify this issue because it can shrink the necessary components of the cochlear implant to fit entirely inside the ear while maintaining its functionality.

2.2 Current State of Research at USZ

Currently, there is no device robust enough to survive the environment of the cochlea, that fits entirely inside the ear, and maintains functionality of traditional implants. (Pffifner et al, 2017). Researchers at USZ are using MEMS technology in their third-generation design of the ICAR working toward their goal of a fully implantable cochlear implant, see Figure 1.

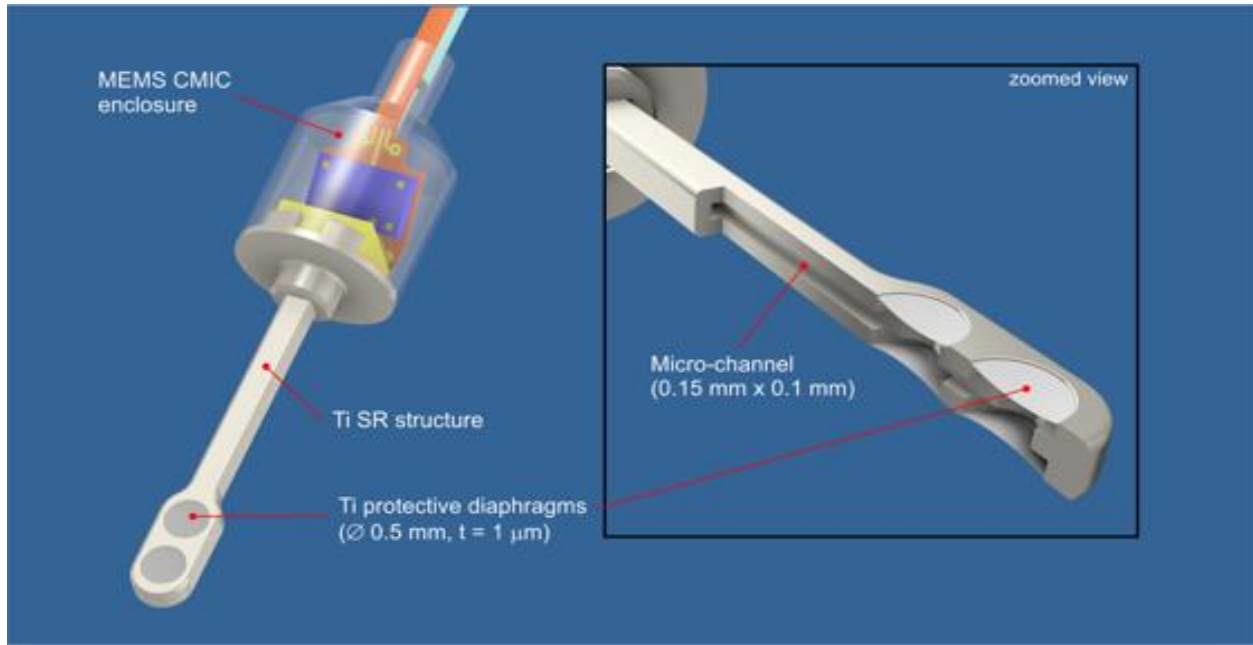


Figure 1: Intracochlear Acoustics Receiver (ICAR) UniversitätsSpital Zurich, (n.d.a).

The ICAR is potentially sensitive enough to measure intracochlear sound pressure (ICSP) which triggers the electrical impulses that are registered by the brain. The device must be biocompatible with the fluid in the cochlea because it is fully implanted in the ear for a human lifetime. Therefore, a major component of the ICAR is the hydrophone, a microphone designed for underwater use.

The researchers at USZ use titanium to produce the sensor of the ICAR due to its extensive lifespan (L. Prochazka, personal communication, August 15, 2018). The sensor consists of three titanium layers with a micro-channel enclosed in the head as illustrated in Figure 1. It also includes protective diaphragms, also referred to as membranes, seen in Figure 2.



Figure 2: ICAR Titanium Layers UniversitätsSpital Zurich, (n.d.b).

These membranes protect the micro-channel from external fluid and provide increased sensitivity. Support material is inserted into the micro-channel before membrane production to keep a constant shape while the membranes are deposited. After the manufacturing process is complete, the support material is removed. This alters the shape of the membranes and provides internal space for vibration registration. As a result, each membrane must pass a three-part quality control inspection to ensure proper function. This inspection determines how different environmental conditions affect the overall shape and sensitivity performance of the sensor-membrane system.

Test I: Quasi-Static Point Load Inspection

The quasi-static point load procedure is completed to measure displacement and Young's modulus of a membrane after a point load is added to the membrane surface. This inspection step utilizes the Micromechanical Testing and Assembly system for FemtoTools at Eidgenössische Technische Hochschule (ETH). In this process, a point force is used to quantify stiffness from force and displacement measurements.

Test II: Acoustic Loading Inspection

The acoustic loading experiment is employed to measure the natural frequency of vibration for the membrane structure. In this process, dynamic diaphragm loading is created by external and internal acoustic stimulation through the application of a pressure load by placing a small repeatable sound source near the membrane. The displacement is measured using one-point Laser Doppler Velocimetry (LDV) and is subsequently used for a stiffness calculation.

Test III: Optical Inspection

During optical inspection, each membrane is observed under a white light microscope to characterize its shape. Images are taken at various increments along the height of the membrane to produce a 3D model of its shape through MATLAB (I. Dobrev, personal communication, August 14, 2018).

The optical inspection procedure is not as developed as the previous inspection steps. The researchers have yet to determine a set of requirements for the ideal membrane shape. Many complete optical inspections will need to be conducted in order to develop Test III. Therefore, the focus of this project is making Test III, the optical inspection of the membranes, more efficient.

2.3 Optical Inspection Overview

Optical inspection can be used as a quality control technique implemented into a manufacturing process to detect defects. This inspection can be completed manually or through an automated machine-based process. An Automated Optical Inspection (AOI) system is customized based on the type of product and inspection technique utilized by the manufacturer. These unique specifications include the type of image capture, lighting, image processing, and software.

AOI image capture provides the options of utilizing a still image camera or streaming video of the product to compare with an ideal sample. The AOI lighting requirements are determined by the composition of the sample and the research guidelines. Lighting options include fluorescent lighting, LED lighting, and infrared or ultraviolet light (“Automatic Optical Inspection”, n.d). To integrate data collection and data analysis, software is implemented for digital image processing. The software required for the AOI process allows for image processing, data analysis, and algorithm development. By using a software that meets these requirements, the researcher is able to precisely measure the size, scale, or the number of objects in a scene. This type of processing can also be used to improve clarity and remove noise in the collected data. (“Process digital images with computer algorithms”, 2018).

Automation of a Microscope for Optical Inspection

Microscopic inspection is becoming increasingly automated to create more efficient processes. Examples of this type of automation are found in cell counting (biological applications) and MEMS device inspection (mechanical applications).

The stage of the microscope is typically the core of the automation process with the critical positioning functions being the XYZ axis movements. The stages contain a lead screw that transmits rotational motion from the dial to the linear distance travelled by the stage. This movement can be driven by stepper motors that provide discrete steps in position (“Microscope Stages” n.d). In comparison to continuous motion motors, stepper motors are able to produce accurate movements at high acceleration and low rotor inertia. It does this by receiving electrical pulses that are programmed and produced through a computer, controller, and driver in a sequence of high or low logic voltage (Stepper Motor Basics, n.d.).

Automation of Membrane Optical Inspection

To obtain images of the hydrophone membrane previously mentioned in Section 2.2, the researchers at USZ isolate one membrane and focus the white light microscope on the surrounding top titanium surface. Then they move the microscope stage 5 μm upward to account for possible curvature of the membrane. Using the fine focusing dial on the microscope, the researchers move the stage down in non-uniform increments to take pictures at various heights of the membrane (See Appendix A). The researchers use Zen, an interactive imaging software, to study and capture images. MATLAB is then used to render a 3D model of the isolated membrane

(L. Prochazka, personal communication, August 15, 2018). This 3D model allows researchers to visualize the full shape of the membrane. This current procedure requires the researcher to operate the microscope for the entire duration of the test. Capturing 15 images takes a researcher approximately 1 hour using this manual process.

As previously stated in Section 2.2, the researchers have yet to determine a set of requirements for the membrane shape. The project team aims to make the image capture and modeling process more efficient through automation of the microscope used for optical inspection. This will allow the researchers to easily gather the data and optimize the post-processing software needed to establish parameters to determine the membrane shape. With these parameters in mind, the researchers will quantitatively be able to characterize whether a membrane is suitable for the intended function of the ICAR.

Chapter 3: Methodology

The optical inspection technique utilized by researchers at USZ can be divided into two main operations; image capture and image processing. The project goal is to design and integrate an efficient automated optical inspection procedure to characterize membrane shape. To attain this goal, the team designed and implemented the hardware needed to control and automate an optical microscope, designed programs for image capture and processing, and conducted tests to further verify and optimize the capabilities of the automated system. The following sections detail the methods for development of the hardware, software, and optimization of the control system. The combined efforts provide the research necessary to develop optical inspection guidelines and deliverables for the researchers at USZ.

3.1 Design and Implementation of Hardware

The optical inspection procedure was automated through the application of a control system (Figure 3). This control system works toward a fully automated inspection procedure by reducing the manual involvement of an operator.

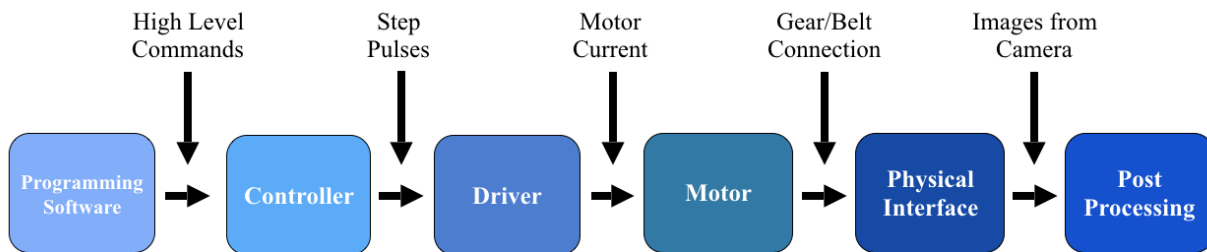


Figure 3: Control System Overview

The team implemented this system on the Leica Microscope used by USZ researchers for membrane optical inspection, see Figure 4. The system moves the microscope stage at precise height increments to focus on different areas of the membrane. The Z-Axis stage moves by turning the fine focus dial on the microscope, number 3 in Figure 4. After each movement, an image is captured with a different area of focus. This is replicated over an established height to capture varying areas of the membrane. The images of the membrane are stacked and processed for shape modelling. A hardware system was designed to interface between the control system and Leica Microscope to precisely and uniformly capture images.

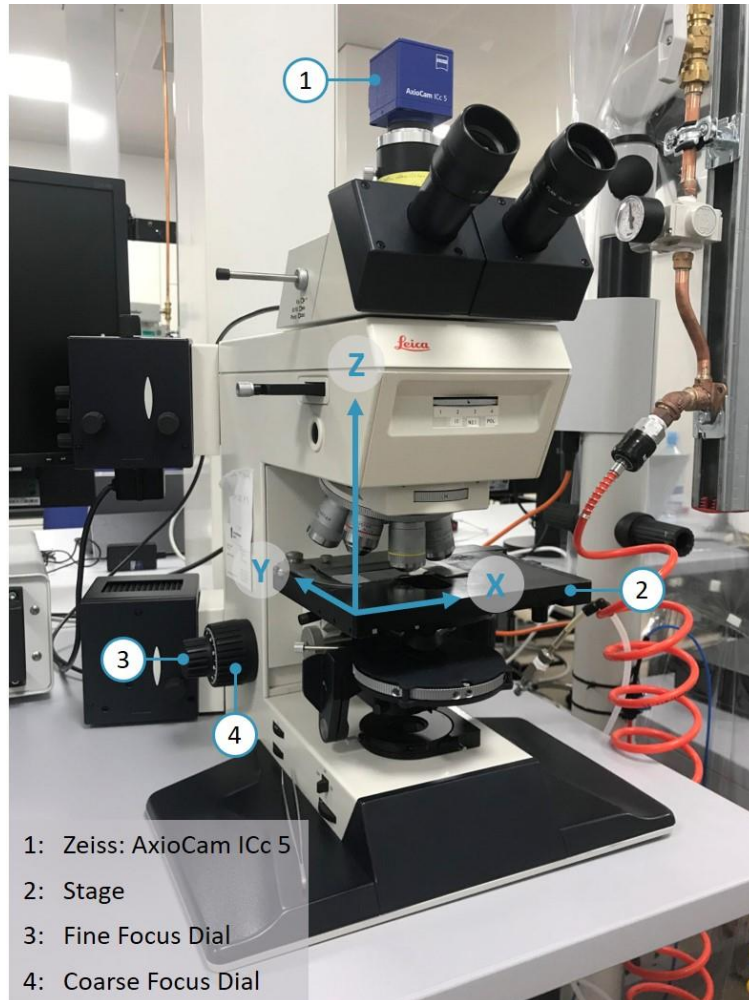


Figure 4: Leica Light Microscope

3.1.1 Z-Axis Control System

The purpose of designing the hardware system was to create a physical interface between the motors and the microscope to automatically control dial and stage movement. The team explored various options for the hardware control system components, designed and constructed preliminary prototypes, and optimized these designs for the final prototype. The following sections describe the physical methods used to automate movement in the Z-Axis.

Control System

The Z-Axis control system is made up of a MATLAB user interface, Arduino Mega 2560 controller, an A4988 stepper driver, and a Makeblock 81042 stepper motor (Figure 5). The control system dictates the rotational movement of the Z-Axis dial which moves the stage vertically in the positive and negative Z direction. This changes the area of focus captured in each image.

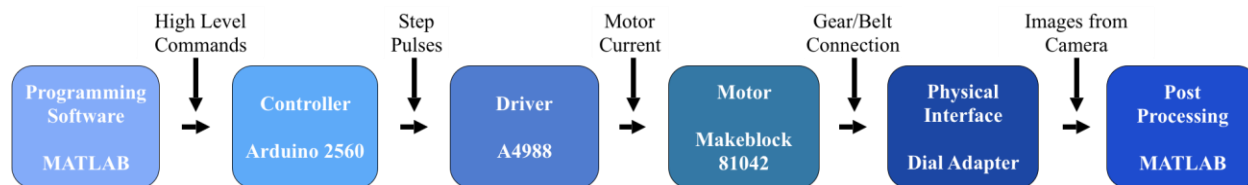


Figure 5: Control System Overview

The physical interface between the stepper motor and the microscope is a mated belt-pulley system that is affixed to the dial. This provides a secure and reliable connection for automation. The team selected a stepper motor over a DC motor because it can move in precise increments, which is ideal for controlled movements. The A4988 stepper driver was chosen because it pairs with the selected controller and motor. The driver is needed to relay commands from the controller to the stepper motor. The team picked an Arduino Mega 2560 as the controller based on its many available digital pin connections for the integration of multiple motors and its compatibility with the MATLAB software. MATLAB was utilized as the programming software because the initial image processing script was coded in MATLAB. This keeps all software in the same programming interface. The team chose to use the AxioCam ICc5 camera for image capture over a USB camera because of its higher resolution. The wiring for the Z-Axis control system can be found in Appendix B. These selected components provided the team with a complete Z-Axis control system for automation and provided a better understanding of system guidelines and limitations.

Proof of Concept Model and Preliminary Prototype

The team created a proof of concept model and preliminary prototype to assess design constraints and determine the necessary materials for a durable system. From this proof of concept model, shown in Figure 6, the team determined the location for the stepper motor in relation to the microscope focusing dial and that the use of a belt-pulley system provided a consistent connection. This model included a stepper motor with grooved timing pulleys, a mated grooved belt, and a support structure consisting of aluminum Makeblock pieces and Legos (Figure 6). The device was connected to the Z-Axis dial via a rubber cover which surrounded the fine focusing dial. The addition of a rubber cover reduced slip more compared to a connection between the belt and the bare dial. This provided the preliminary physical interface between the stepper motor system and the stage movement.

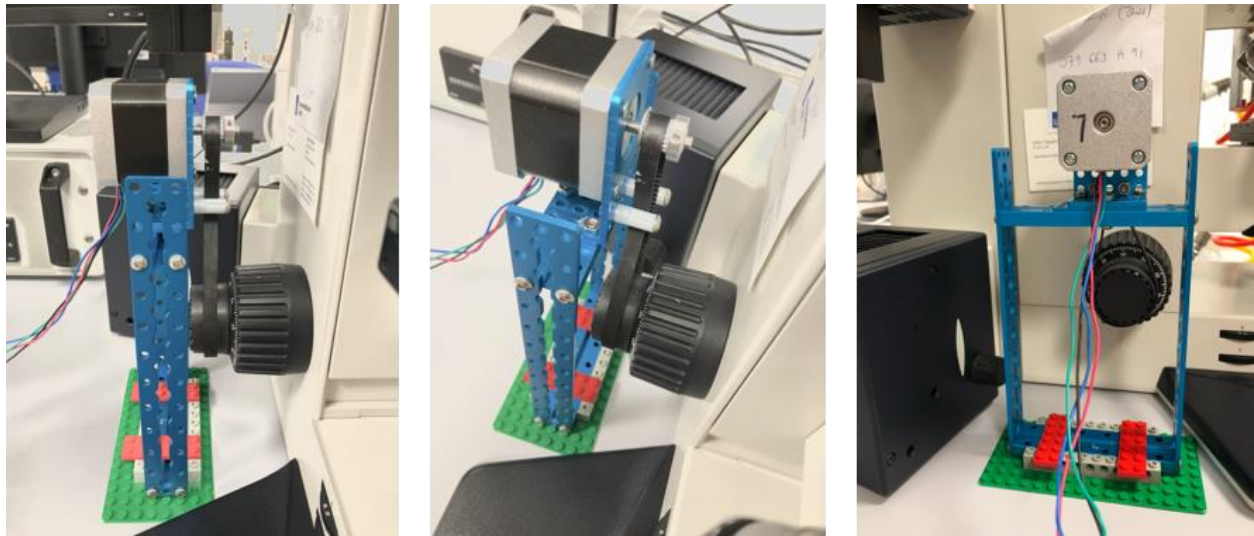


Figure 6: Z-Axis Control System Proof of Concept Model

In the development of this proof of concept model the team learned explicit design constraints and requirements for the connection of the stepper motor to the Z-Axis dial. Fundamental design constraints include the necessity to have a compact control system, which fits in the limited space at the microscope station, and to place the motor so the belt is sufficiently taught. Additionally, it is a requirement to have a detachable dial connection due to the microscope's role in many research settings.

Prototype I, developed based on the learnings from the proof of concept, introduced a more robust physical connection with the mated gear-pulley system attached to the Z-Axis dial and the stepper motor (Figure 7). The goal of this improvement was to translate uniform motor steps to the dial. The team added blue aluminum alignment pieces on both sides of the pulley to keep the belt from detaching, as seen in Figure 7. The support for the motor was improved by using two optical post assemblies and a universal stage made by ThorLabs. A 3 mm thick piece of vibration isolating material was placed under the universal stage to reduce vibration and slip between the stage and table. Material was added on the inner surface of the dial adapter to increase friction and create a better surface connection between the 3D printed cylindrical adapter and the focusing dial.

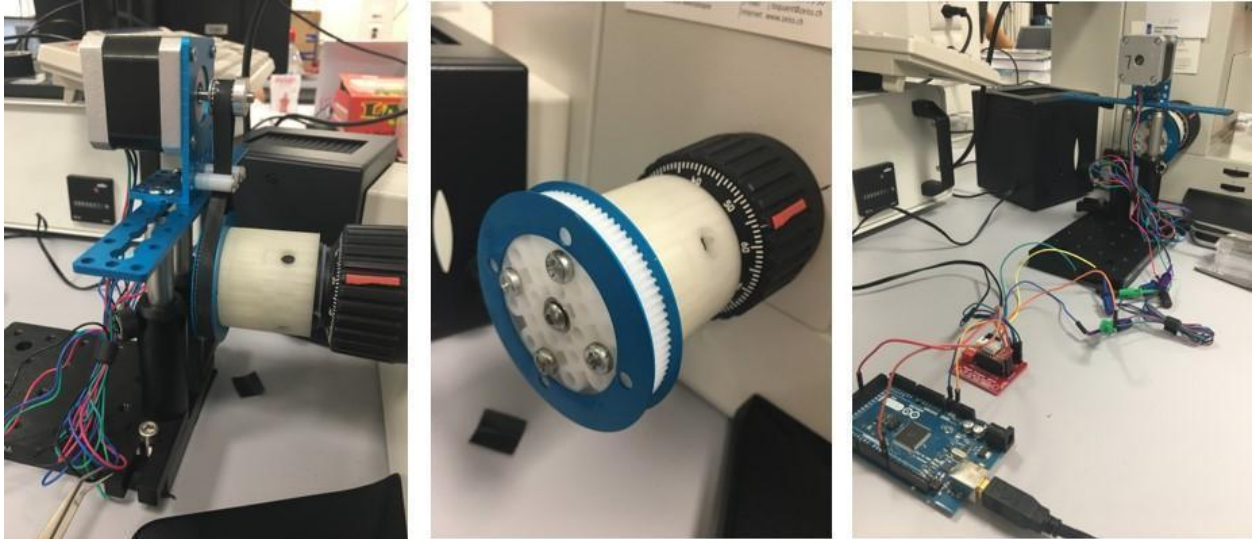


Figure 7: Z-Axis Control System Prototype I

The four-screw mounting configuration used to clamp the adapter to the focusing dial in Figure 8 did not provide a sufficiently aligned connection to the surface. This allowed for slip and movement of the dial adapter during testing.

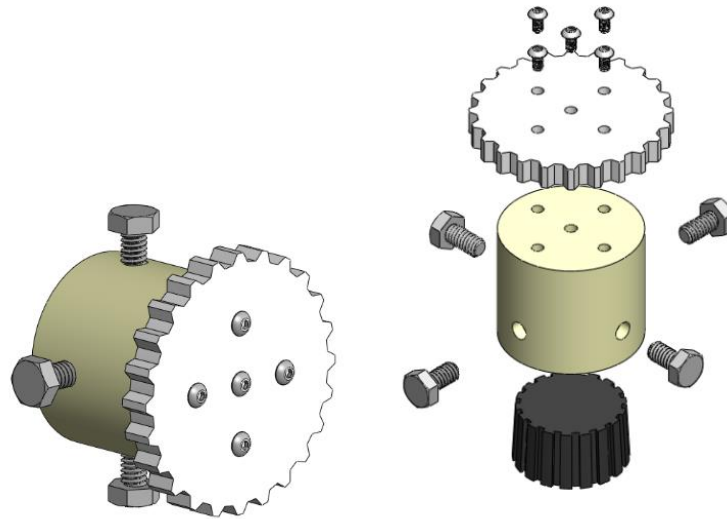


Figure 8: Z-Axis Dial Adapter CAD Model

The team drilled three new holes into the dial adapter to form a kinematic clamp configuration. With three points of contact, it was difficult to equally insert all of the bolts to fully engage and center the dial. These preliminary prototypes made the various design limitations and potential mechanical issues evident for the final design needed to automate Z-Axis movement.

Final Design

The primary concern with Prototype I was that the dial adapter did not create a reliable connection. Therefore, the team designed Prototype II with an optimized dial adapter based on commercially available pipe clamps. As seen in Figure 9, this design has two mating pieces. The inner piece includes wedges that are semi-flexible at the base. The outer cylindrical piece surrounds the wedges to ensure the inner piece remains captive to the dial. Tightening the four screws forces the wedges against the opposing surface of the dial and the outer cylindrical piece, fully clamping the adapter to the dial in the process. Similar to the previous design, the pulley is then mounted to the surface of the adapter.

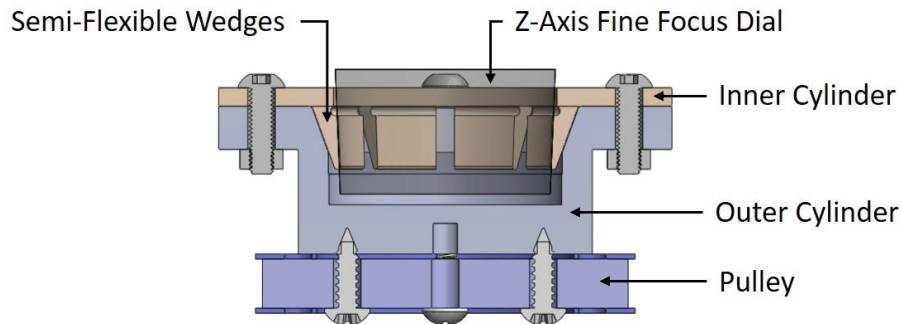


Figure 9: Z-Axis Dial Adapter Final Design CAD Model

The inner and outer cylindrical pieces were manufactured through 3D printing and performed as intended. The mated belt-pulley system was then attached to the end of the adapter to create a constant and reliable connection to the other components of the Z-Axis control system (Figure 10).

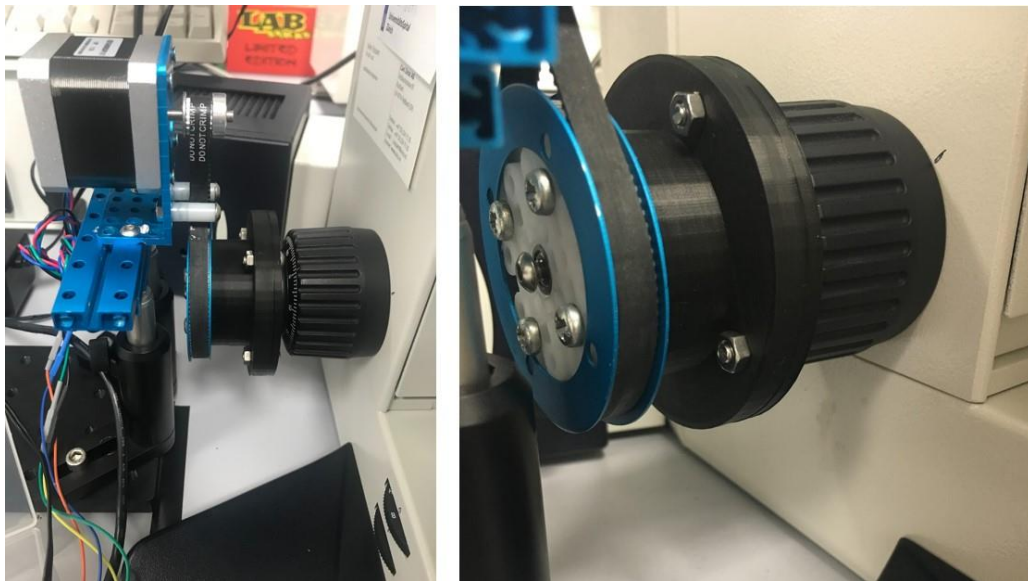


Figure 10: Z-Axis Dial Adapter Final Design

3.1.2 X and Y Axis Control System

Automation of the Z-Axis allows the control system to inspect a single membrane. To automate the entire inspection process, X and Y Axis control is needed to move between all membranes in the sample holder, shown in Figure 11. While researchers are not yet inspecting entire sample holders of sensor head membranes, having the necessary control system components in place for implementation will allow inspection to be fully automated for future use (L. Prochazka, personal communication, August 15, 2018).

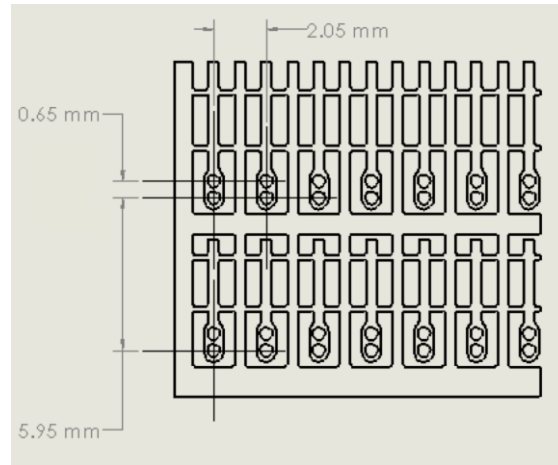


Figure 11: Distance between membranes in a sample holder

Control System

The X and Y control system has two motors, one for X and one for Y movement. It uses the same programming software and controller, but has separate drivers and physical interfaces for each motor, seen in Figure 12.

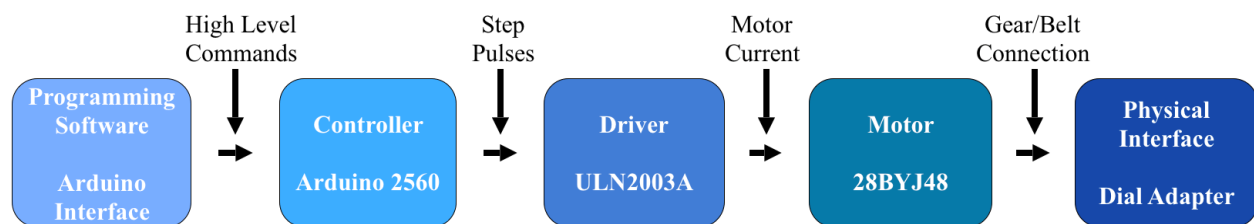


Figure 12: X and Y Axis Control System

The control system uses 12V DC 28BYJ48 stepper motors to control the X and Y Axis movements of the automated microscope. These motors are designed to be mounted and are lighter than the Z-Axis motor for ease of integration. To incorporate one power source for both motors, a breadboard was used with a 9V power source. To program movements in MATLAB, the Arduino library must be used. The motors were programmed with the Arduino user interface for preliminary investigations. The wiring for the X and Y Axis control system can be found in Appendix C.

Preliminary Prototype

Similar to the Z-Axis, the team decided to use the existing X and Y dials of the microscope to move the sample. The physical interfaces are removable because the microscope is required to be functional for purposes other than membrane optical inspection. These dials are attached to the stage; therefore, the motors have to move with the stage. Additionally, the dials are stacked axially yet move independently as shown in Figure 13. These observations provided design constraints for the dial adapters and motor placement.

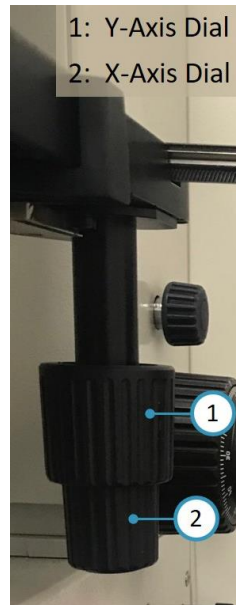


Figure 13: X and Y Axis Dials on Leica Light Microscope

The belt and pulley system used for Z-Axis control was also used to attach motors to the X and Y dials. This required the pulleys to be mounted to the dials and the motors to be aligned parallel to the pulleys.

All prototypes include two components: a motor housing and a dial adapter to mount the pulleys on the dials. The first component provides a support structure to position the motors parallel to the dials. The second component mounts the pulleys around the dials and holds a constant position for a uniform connection when the mating belt is used. The two components allow a belt to be connected between the motors and the dials to transfer and control motion.

Housings to mount and position the motors were based on the design constraints of the X and Y dial locations. Two 12V DC 28BYJ48 stepper motors were used because of their smaller size, lower weight, ability to be fixed on a surface, and for the ease of independent control. The motors, seen in Figure 14, weigh 40 grams and are able to be mounted with a 35 mm distance between through holes (Schrittmotor, n.d.).



Figure 14: X and Y Axis Stepper Motor (Schrittmotor, n.d.)

Design I to position the motors, seen in Figure 15, includes a clamping feature to the microscope stage. This design provides mounting surfaces to position the motors parallel to the dials. From this, the team observed that the motor housings should be an adjustable structure. This would keep the motors at a distance where the belts would be taught at all times. Design I also included the four-bolt design as mentioned in Section 3.1.1, Figure 8, for the X and Y dial adapters. However, with the lack of proper alignment onto the dials, the team considered other methods of connecting cylinders-to-cylinders.

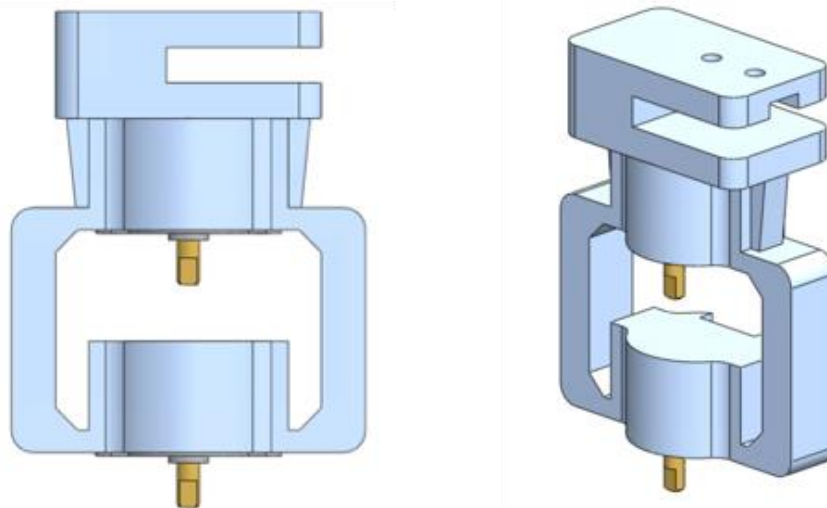


Figure 15: Design I - Stepper Motor to Microscope Stage Clamp

Design II incorporated the same motor housings and a different dial adapter design. The new dial adapters utilized a hose clamp above and below the pulley to hold the gear in place on the dials, see Figure 16. However, this would require a larger surface area for clamping making it difficult to fit all components on the dial axis.

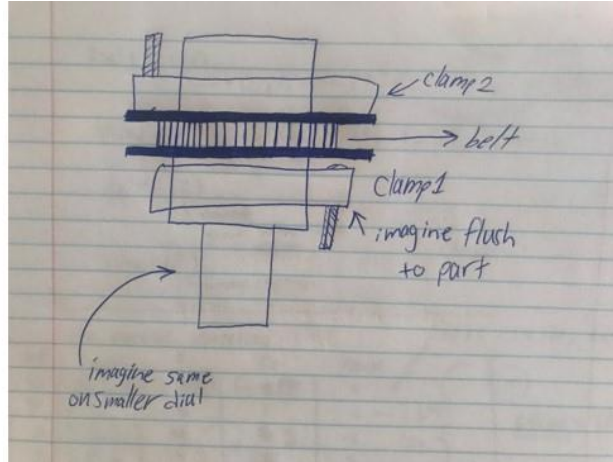


Figure 16: Design II - Preliminary X and Y Axis Dial Adapter Design with Hose Clamp Implementation (Cade, n.d.)

From the observations in Design I and II, a new design (Figure 17) was generated to use ThorLabs pieces to clamp to the stage and provide a vertical axis. This allows for adjustable positioning of the motors and housings.

Final Design

The motor housing component of Design III fulfilled the idea of having both motors on the same adjustable structure to align with the dials. This also allows for the motors to be moved to sufficiently tighten the belts around the timing pulleys. The assembly of the two motor housings, ThorLabs optical posts, and angle clamps can be seen in Figure 17. The motor housings were designed to fit around ThorLabs angle clamps which are made to secure to the optical posts. The addition of the motor housings allows the motors to be mounted independently in stable positions.

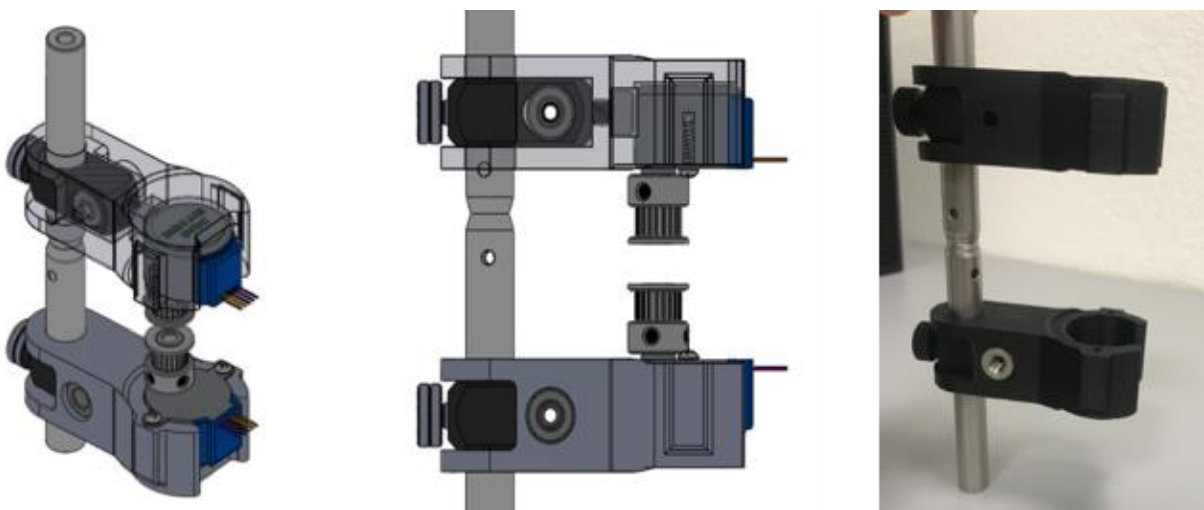


Figure 17: Design III - Motor Housing CAD Models (left and middle) and 3D Printed Models (right)

The X and Y dial adapter component for Design III is seen in Figure 18. This uses the same clamping method as the final design of the Z-Axis dial adapter to provide a secure fit around the dials while being removable for other uses of the microscope. Alterations were made to this design to fit the dimensions of the X and Y dials and prevent interference between each dial adapter because of the positioning of the screws. Due to the configuration of the X and Y dials, the pulleys needed to be positioned around each dial, unlike the Z-Axis configuration which has the pulley adjacent to the focusing dial.



Figure 18: Design III - CAD Models of the X and Y Axis Dial Adapters (left and middle) and Final Dial Adapters (right)

The application of Design III for the motor housing and X and Y dial adapters is seen in Figure 19. This includes the belt-pulley setup for further automation of the inspection process for the entire sample holder.

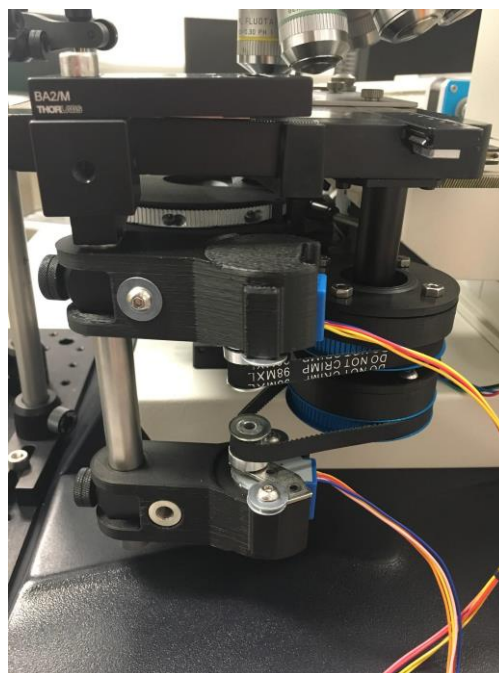


Figure 19: Design III - Motor Housing and Dial Adapters for X and Y

3.2 Design of Image Capture and Image Processing Scripts

MATLAB scripts were developed to program the image capture and processing procedures with the implemented hardware. The image capture and processing scripts were developed through the use of block diagrams and procedures as described in the following sections.

3.2.1 Image Capture Script

The first procedure of the optical inspection process includes the automatic capture and saving of images. This is completed through automatically turning the microscope dial uniformly to capture and save images at specified increments of distance between pictures, known as the slice resolution (Figure 20).

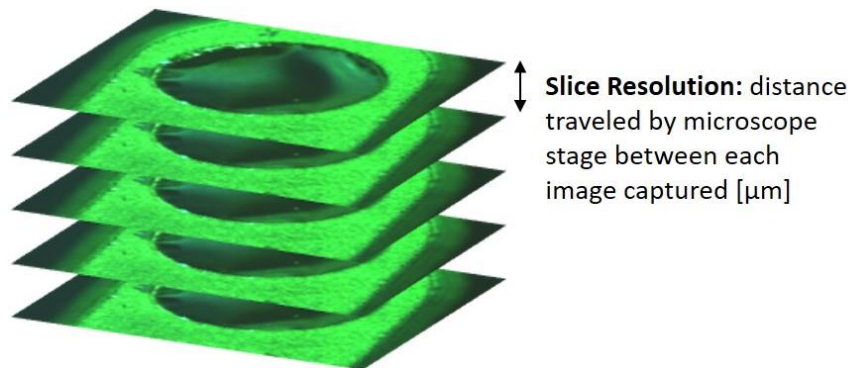


Figure 20: Slice Resolution Visual Definition

The turning of the dial controls the movement of the stage in the Z-Axis, changing where the focus of each image is. The block diagram in Figure 21 illustrates the image capture script along with a description of the process in Table 1. This script provides the high-level commands that come from the programming software block in Figure 5. This controls the Arduino Mega 2560, the A4988 driver, and the Makeblock 81042 stepper motor, thereby moving the physical interface for microscope control. These are the first five blocks illustrated in Figure 5.

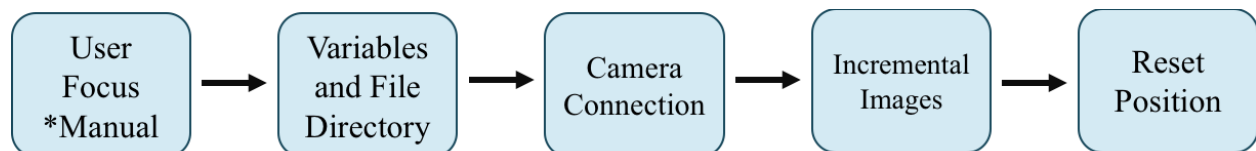


Figure 21: Overview of Image Capture Procedure

Table 1: Overview of Image Capture Procedure

Overview of Image Capture Procedure
<p>User Focus: User focuses the microscope on the top titanium layer of the membrane structure by using the Data Acquisition toolbox window and a preview of the image as seen through the camera.</p> <p>* The rest of the procedure is operated with MATLAB.</p>
<p>Variables and File Directory: Using MATLAB prompt boxes, the user assigns a base name for images, a folder path for image saving, image capture color scale, total height span for image capture, and the linear distance traveled by the microscope stage between images.</p>
<p>Camera Connection: The MATLAB script creates a connection for communication between the camera and the Arduino. This script also notifies the user when the connection has been established. This reduces the risk of lost time if the camera does not connect properly for image capture.</p>
<p>Incremental Images: Within a loop, the script uses the playTone function to send commands to the motor for stepping, then pauses while an image is captured and saved, and pauses again for the start of the next loop.</p>
<p>Reset Position: Once the images are captured throughout the specified height, the motor reverses direction to return the stage to a home position before moving to the next membrane.</p>

3.2.2 Image Processing Script

The second procedure of membrane optical inspection processes the images captured during the first procedure to generate plots that are representative of the membrane shape. These plots are generated using methods similar to image stacking. The files are organized in ascending order and read by the script to calculate the focus of each individual image. This data is then used to create a shape that is representative of the membrane. The shape is filtered to remove any noise to generate the final plots for data analysis. To make measurements from the final plots, the script requires the following inputs: slice resolution, cell radius, and cell pitch. The slice resolution is the interval distance [μm] between each captured image. A cell is a group of pixels averaged together to calculate the focus of an image. The cell radius is representative of the number of pixels in a cell and the cell pitch is the distance between cell centers (see Figure 22).

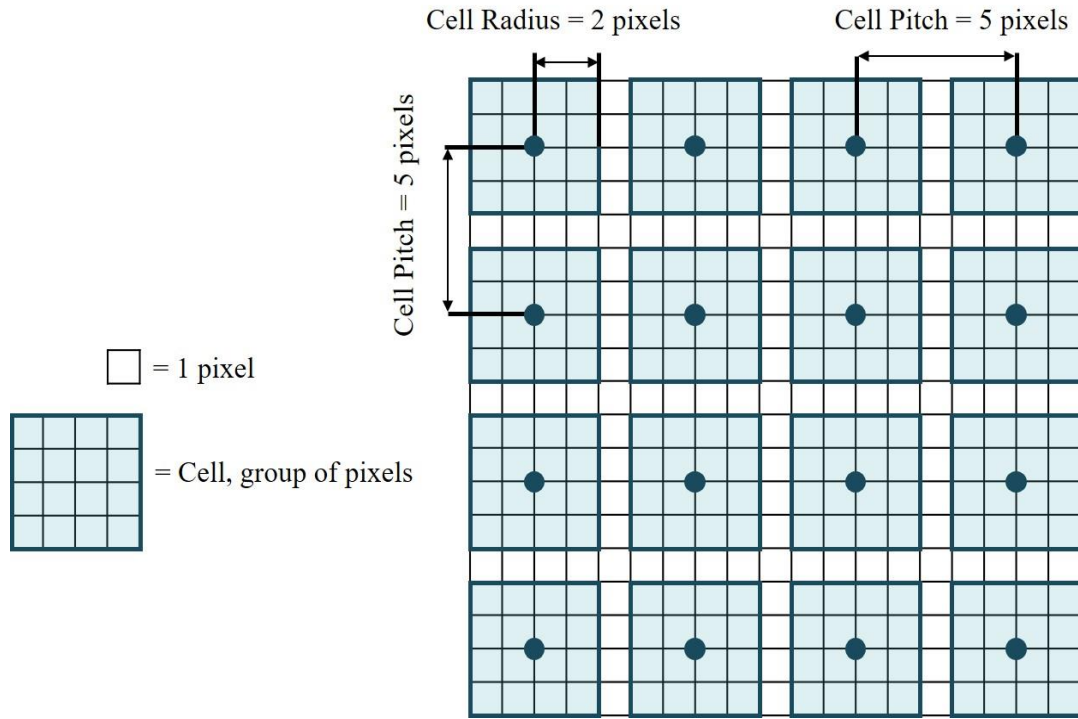


Figure 22: Cell Radius and Cell Pitch Example (figure not to scale)

The block diagram illustrated in Figure 23 represents the overall components of the image processing script and Table 2 includes the individual steps executed. The components of this block diagram are an expansion of the post processing block of the Z-Axis control system seen in Figure 5.

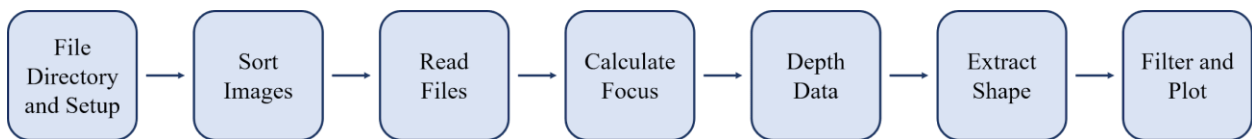
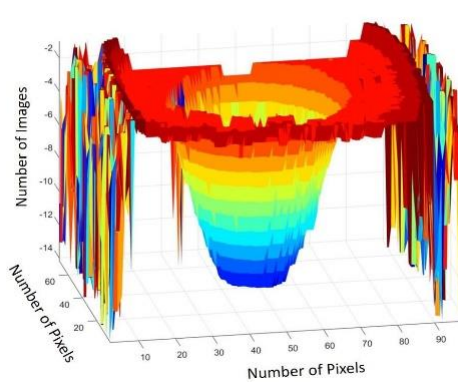


Figure 23: Overview of Image Processing Procedure

Table 2: Overview of Image Processing Procedure

Image Processing Procedure
File Directory and Setup: the location of the images captured during module one, the slice resolution, cell radius, cell pitch, and image base name are set up in the script by the user.
Sort Images: images are sorted in ascending order by the number after the base name to ensure images are stacked correctly.
Read Files: files are read by the script before processing.
Calculate Focus: for individual images, the pixels are grouped and averaged into cells (based on cell radius and pitch inputs). These cells are then assigned a numerical focus value.
Depth Data: the images, with newly assigned numerical focus values, are stacked together to create a height cube.
Extract Shape: the data in the height cube is used to create a shape representative of the membrane by relating the focus values to height in reality.
Filter and Plot: the previously generated shape is filtered to remove noise from the data to generate plots representative of the membrane shape, illustrated below.



3.3 Verification and Optimization of Control System

Experiments were designed and completed to test the functionality of the control system. This included testing the capability of producing output measurements that are representative of the actual membrane shape. Subsequent testing provided insight into ideal conditions and parameters for data analysis. Through this testing the team was able to verify and optimize the control system.

3.3.1 Investigation of Potential Physical Error

The team observed and reduced potential sources of physical error to optimize the Z-Axis system. The identified areas for possible sources of error included: vibrations, slip, wiring, power supply, and motor performance. These potential areas of physical error were addressed prior to further testing.

The stepper motor demonstrated throughout testing that vibrations from the system affect the table where the microscope is located. These vibrations could transfer to the microscope and affect the quality of images captured during optical inspection. The team observed the need for a no slip grip between the belt and pulley to ensure proper transfer of motion between the motor and dial for correct image capture. During prototyping, all electrical connections were made using wire testing hooks and electrical wire. The team observed disrupted communication within the system due to misconnected wires, which caused the motor to not move. Also, the team used a power source of a rechargeable 9V battery for preliminary system testing. This was observed to be unreliable as the battery would discharge over time and not provide sufficient voltage. This observation highlighted the need for a consistent power source to reduce error in motor movements.

To ensure maximum grip of the belt and pulley system, the chosen belt includes compatible teeth on the side that has contact with the pulleys. This minimizes the possible slip between the two components.

During prototyping, all electrical connections were made using wire testing hooks and electrical wire. To account for floating wires, connections without proper electrical communication, all wire connections were soldered and reinforced with heat-shrink tubing. A compounding source of error is the possibility for disconnected or misplaced wires from improper system setup and storage. To minimize the possibility of any system wiring disruptions, the team developed housing components for consistent storage and setup of all electrical components.

The team used a power source of a rechargeable 9V battery for preliminary system testing. This proved to be unreliable as the battery would discharge over time and not provide sufficient voltage. To mediate this, a 15V wall power supply with constant voltage output was implemented.

The performance of the motor was evaluated by testing its ability to move and return to its original position. An experiment was carried out by moving the stage down a specified distance (1), then up to past its starting point (2), and then to the original starting point (3) (Figure 24). To measure the end offset of the motor, a Mahr Millimes 1003 micrometer was used to measure the starting position of the stage and its final position (see Figure 24). This procedure mimics the movements of the motor during the image capture process and removes the variable of hysteresis in testing. This test was replicated three times for the different slice resolutions available (Table 3).

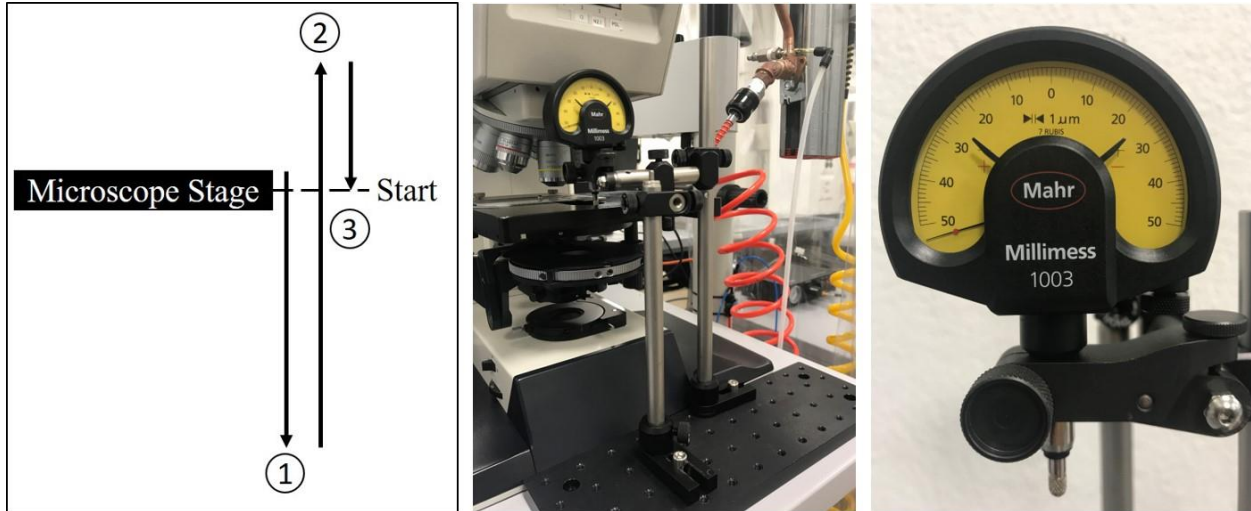


Figure 24: Stage Offset Testing Procedure (left), Stage Measurement Setup (middle) and Mahr Millimess Micrometer (right)

Table 3 shows the corresponding number of units needed to travel a specified distance in terms of micrometers used to develop the testing matrix. A unit is defined as the number of corresponding motor steps needed to achieve a slice resolution, an example is seen in Figure 25.

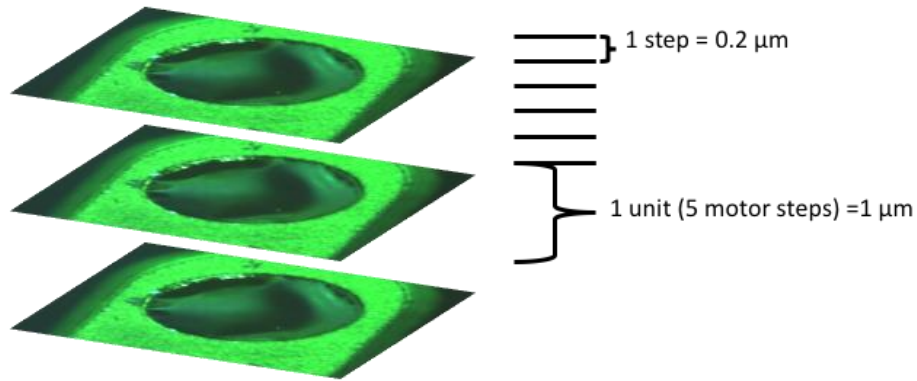


Figure 25: A 1 μm slice resolution unit equals 5 motor steps

For slice resolutions of 0.6 μm and 0.8 μm the distances traveled for the downward, upward, and return movements were adjusted to the nearest integer of motor step units. For example, a slice resolution of 0.8 μm can travel a distance of 30 μm if the number of units traveled is 37.8, this was adjusted to 32 μm an equivalent of 40 units.

Table 3: Distance to Travel per Direction for each Slice Resolution

	Slice Res = 0.2 μm		Slice Res = 0.4 μm		Slice Res = 0.6 μm		Slice Res = 0.8 μm		Slice Res = 1 μm		Slice Res = 2 μm	
	μm	# of Units	μm	# of Units	μm	# of Units	μm	# of Units	μm	# of Units	μm	# of Units
Down	30	150	30	75	30	50	32	40	30	30	30	15
Up	40	200	40	100	42	70	40	50	40	40	40	20
Return	10	50	10	25	12	20	8	10	10	10	10	5

3.3.2 Establishment of Control System Characteristics

The implemented Z-Axis control system and image capture procedure provided a basis for an automated inspection process. Once areas of physical error were investigated, standardization and calibration investigations were conducted to establish the control system characteristics.

Magnification Level for Optical Inspection

The team investigated available magnification values for optical inspection to select standard settings for uniform image capture to compare membrane data. The values tested were the 5x, 10x, and 20x magnification levels due to the differences in field of view. To complete this study images at the different magnification levels were captured using the AxioCam ICc5 camera. The differences investigated were the number of membranes that appear in the field of view along with the clarity of image capture at that magnification level.

Equation of Pixel Size to Physical Measurements

The image processing software generates models of the membrane curvature in terms of pixels. These pixels are later equated to microns to make data measurements. The relationship between pixel size and microns was calculated from the images, captured by the AxioCam ICc5, that show the calibration tool in the field of view. The team used a calibration ruler with divisions of 10 μm to measure the physical size of a 2452x2056 pixel image, the standard image size used across all membranes. Both the width and height of the image were measured using the calibration ruler to verify the pixel size.

Calibration of Z-Axis Dial Movement

The goal of calibrating the Z-Axis dial movement was to ultimately relate stepper motor steps to the linear distance travelled by the microscope stage. To do this, the relationship of the motion of the motor, dial, and stage needed to be determined. The only known correlation is provided in the Leica microscope manual which states, “one division of the scale represents a vertical (stage) movement of approx. 2 μm ” (Leica, 1999, p.57). These dial divisions are shown in Figure 26. The calibration for the Z-Axis dial was completed both manually and automatically.

Manual Calibration

The manual calibration related the rotational movement of the dial to the linear distance traveled by the microscope stage. The calibration was completed to verify the relationship stated in the manual for the Leica Light microscope, due to it being an approximation.



Figure 26: Z-Axis Coarse and Fine Focusing Dials of Leica Light Microscope

This was completed by using one layer of the sensor head's titanium structure as a measuring device. Each layer is specified by the manufacturer to have a thickness of $100\ \mu\text{m}$ with no provided tolerance (ATI Flat Rolled Products, 2015). When the membrane is not present in the sample, the top and middle titanium layers can be viewed and focused on with the microscope, as seen in Figure 27. The dial increments spanned between when the microscope is focused on the top and middle layers can then be related to distance.

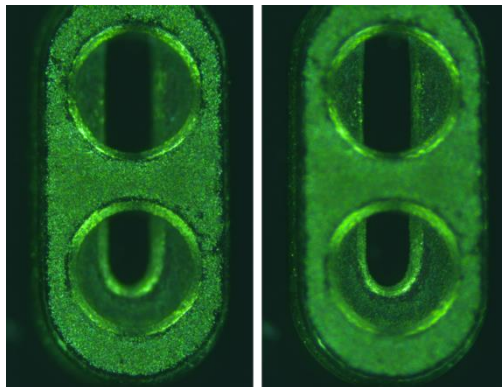


Figure 27: Top (left) and Middle (right) Titanium Layers

To relate the dial increments to distance, the operator first turned the dial to focus on the top titanium layer (Figure 27) and recorded the position. The operator then focused on the middle titanium layer (Figure 27) and recorded the new dial position. This was repeated three times for each sensor head and replicated on five total samples by two different operators. The $0.1\ \text{mm}$ distance was divided by the difference of the dial increments from the focused layers and then multiplied by 1000 to convert the measurement to micrometers. This familiarized the team with the relationship between the dial movement and microscope stage, but did not include results to describe the stepper motor movement control of the stage.

Automated Calibration

The relationship between the rotational movement of the stepper motor and linear distance traveled by the stage was verified using the automated control system. The manual calibration was used to verify the ratio between dial increments and linear distance traveled by the microscope stage (Ratio A). The automated calibration applied the mathematical relationship of stepper motor steps to distance traveled by the microscope stage (Ratio C). To calculate the relationship, the ratio between stepper motor steps and dial increments needed to be determined (Ratio B). The culmination of Ratio A and Ratio B then related stepper motor steps to linear distance of the stage.

Ratio A = Dial Increments : Linear Distance of the Stage

Ratio B = Stepper Motor Steps : Dial Increments

Ratio C = Ratio A + Ratio B = Stepper Motor Steps : Linear Stage Distance

After developing the ratios described above, the mathematical calculations were applied within the MATLAB script during the testing procedure described in Table 4 and Figure 28. The automated image capture control system and processing script were used to complete this investigation. This testing measured the thickness of one titanium layer within the sensor structure which has a known value of 100 μm (ATI Flat Rolled Products, 2015).

Table 4: Titanium Layer Thickness Verification Procedure

Titanium Layer Thickness Verification
Step 1: User focuses the microscope on the top titanium surface.
Step 2: The image capture script moves the stage 2 μm upward to account for user error. The image capture script then scans a total of 4 μm taking images at increments of 0.2 μm .
Step 3: The stage is then moved 96 μm without any image capture.
Step 4: The image capture script then scans a total of 4 μm taking images at every 0.2 μm .
Step 5: The captured images are processed using the image processing script. A plot is outputted showing the quantified focus values over the distance traveled. The distance between the first maximum focus value (location of the top titanium layer) and last maximum focus value (location of the middle titanium layer) is found.

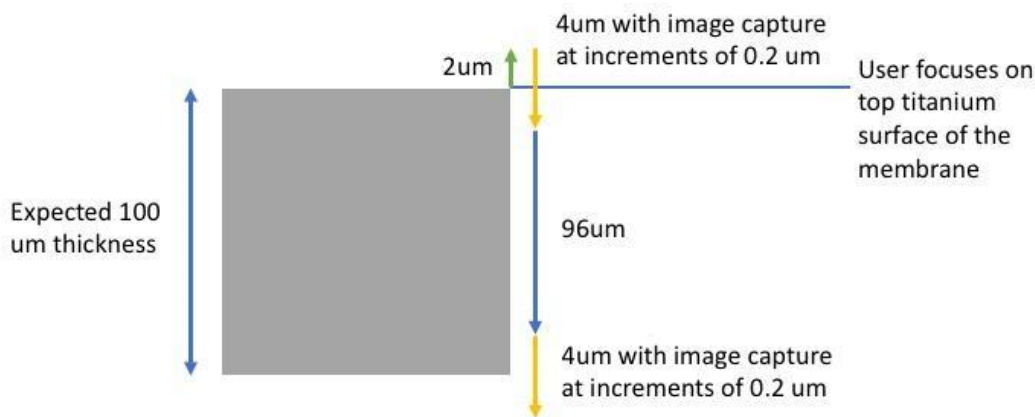


Figure 28: Graphical Representation of Titanium Layer Thickness Verification Procedure

Calibration of X and Y Axis Dial Movement

To achieve fully automated optical inspection the procedure for the Z-Axis must be integrated with movements in the X and Y directions. The team conducted preliminary investigations to relate the number of motor steps needed to transverse the sample holder (Figure 11) for movement between membranes. To complete the investigation, each 28BYJ48 stepper motor was programmed and controlled through the Arduino interface. The AxioCam ICc5 and the Data Acquisition tool in MATLAB were used to preview the positioning of the sample holder. The test began by manually centering and aligning a membrane sample within the camera frame. The motor was moved by providing a number input for stepper motor steps to bring the center of subsequent membranes into view. The motion of the motor was transferred to linear motion of the stage through the belt and pulley system described in Section 3.1.2. Once each sample was centered in the camera preview, the steps inputted in the program were totaled to provide the researchers with approximate values for X and Y movement during complete automation.

Measurement Parameters for Membrane Shape Comparison

Parameters of height and diameter were used to quantitatively compare membranes. This supplements qualitative membrane characterization and inspection. These parameters were used to measure the effect of different MATLAB inputs on the output graphs. The team standardized the method for measuring membrane diameter and height to determine which of these parameters could be used to compare membrane samples quantitatively.

The image processing MATLAB script generates a 2D plot to measure diameter and height across all membrane samples. The plots are generated by analyzing a cross-section of the stacked images across the horizontal center. Pixel size and slice resolution directly affect the scaling of the plot axes and subsequently the membrane characterization measurements. An example 2D plot is illustrated below for a slice resolution of $0.4 \mu\text{m}$ and standard pixel size of $2.9 \mu\text{m}$. The plot is annotated with three data cursor points for calculations of height and diameter as seen in Figure 29.

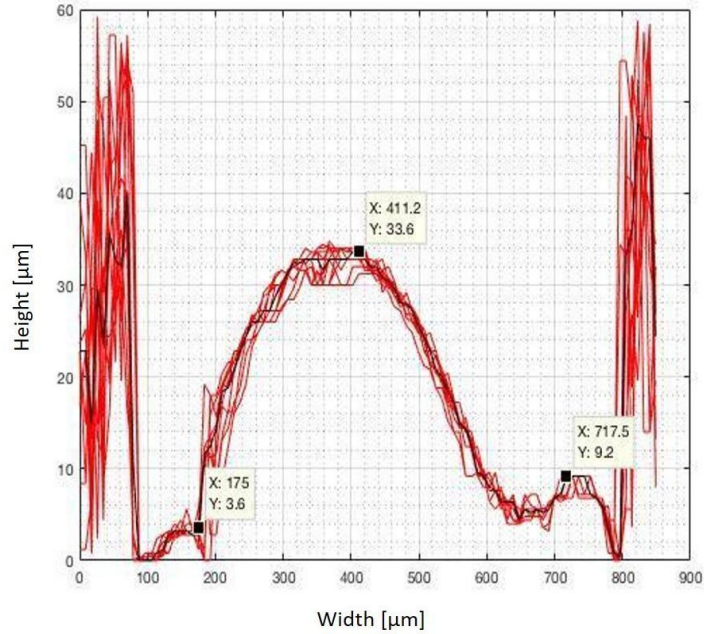


Figure 29: 2D Plot of Membrane Curvature with Data Cursors

Diameter Calculation:

$$D = X2 - X1 = 717.5 - 175 = 542.5 \mu\text{m}$$

Height Calculation:

$$H = Y2 - Y1 = 33.6 - 3.6 = 30 \mu\text{m}$$

All diameter and height calculations were based on characteristic peaks and valleys seen in the 2D plot. This allowed the team to compare data from each 2D plot by using characteristic features as references.

The team investigated the effects of measuring a membrane at different cross-sectional areas to understand how the misalignment of the sample holder affects diameter and height measurements. Three membrane samples were tested at the cross sections seen in Figure 30.

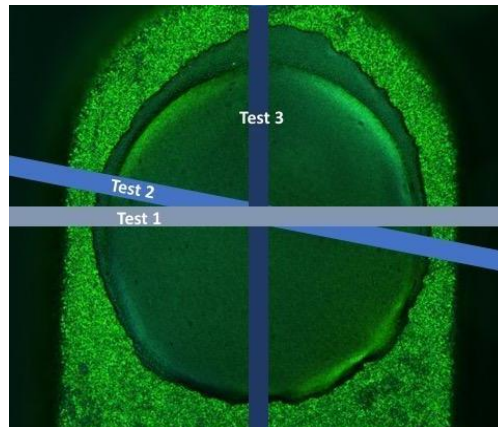


Figure 30: Membrane Cross Sectional Area Tests

3.3.3 Optimization of System Functionality

The team established uniform parameters for image collection and processing by completing several tests to optimize the possible variables and test setups. The image collection optimization included a Design of Experiments for the development of control system presets. The image processing optimization included testing to develop measurement parameters and inputs for image analysis.

Design of Experiments for Image Capture Presets

A Design of Experiments (DOE) was developed to quantify the potential influence of setup factors on the accuracy of the motor during the image capture process. These factors served as MATLAB inputs for the playTone function for each available slice resolution. The playTone function is used to communicate stepping commands between the MATLAB program and the Arduino controller. This function requires input values for frequency and duration. The frequency can range from 0 to 32,767 Hz and the duration can range from 0 to 30 seconds. The product of the frequency and duration values directly correlates to the number of motor steps, as described in Table 5. For example, a frequency of 2 Hz and a duration of 5 seconds yields 10 motor steps. Inversely, a frequency of 5 Hz and a duration of 2 seconds also yields 10 motor steps. The number of corresponding motor steps needed to achieve a slice resolution is referred to as a unit. After each unit, the program is paused to allow the motor to complete the specified steps before an image is captured. The addition of a pause ensures commands are not overwritten as the Arduino receives and executes them.

Table 5: Corresponding Motor Steps to Slice Resolution

Slice Resolution	Unit (Frequency*Duration)
0.2 μm	1 motor step
0.4 μm	2 motor steps
0.6 μm	3 motor steps
0.8 μm	4 motor steps
1 μm	5 motor steps
2 μm	10 motor steps

The DOE tested two factors; frequency and duration as well as pause between units, to determine the ideal settings for each possible slice resolution.

The hypotheses of this experiment were twofold:

1. Pause: This factor will not have an effect on the offset of the total distance traveled by the microscope. It will only affect the efficiency of executing commands.
2. Frequency and Duration: This factor will have an effect on the offset of the total distance traveled because of the acceleration from the constant start-stop movements of the stepper motor.

Testing was completed by measuring the offset [μm] from the expected distance of travel. The combinations of factors for frequency and duration must have a product of the number of motor steps between each image, as shown in Table 5. The DOE frequency (F) and duration (D) combinations are illustrated in Table 6. Each configuration was tested against two possible options for pause; 2 and 5 seconds.

Table 6: Frequency and Duration Configurations

Unit	Slice Resolution	Combination 1		Combination 2		Combination 3		Combination 4	
		F (Hz)	D (sec)	F (Hz)	D (sec)	F (Hz)	D (sec)	F (Hz)	D (sec)
10 steps	2 μm	1	10	2	5	5	2	10	1
5 steps	1 μm	1	5	5	1				
4 steps	0.8 μm	1	4	2	2	4	1		
3 steps	0.6 μm	1	3	3	1				
2 steps	0.4 μm	1	2	2	1				
1 step	0.2 μm	1	1						

An example DOE test matrix is illustrated in Table 7. Each group of testing configurations was replicated to ensure repeatability of results. The testing matrices were developed utilizing the Minitab18 software for each slice resolution described in Table 5.

Table 7: DOE for Frequency/Duration and Pause Configurations

↓	C1	C2	C3	C4	C5	C6	C7 <input checked="" type="checkbox"/>	C8
	StdOrder	RunOrder	CenterPt	Blocks	F.D	Pause	Offset	Time
1	7	1	1	1	1.2	5	0.2	12.0
2	4	2	1	1	2.1	5	0.1	12.0
3	3	3	1	1	1.2	5	0.5	12.0
4	6	4	1	1	2.1	2	0.0	5.5
5	5	5	1	1	1.2	2	0.0	5.5
6	1	6	1	1	1.2	2	0.0	5.5
7	2	7	1	1	2.1	2	0.1	5.5
8	8	8	1	1	2.1	5	0.0	12.0

The standard order (C1) refers to a non-randomized testing order. The run order (C2) refers to the order in which Minitab recommends testing completion. The center point value (C3) of 1 means a high or low value is used in each setup and the block number (C4) of 1 for every test run means all testing should be completed under the same environmental conditions (“How Minitab Stores Design Information”, 2017). The F.D combination (C5) refers to the frequency and duration values with the naming convention of [Frequency.Duration]. The pause (C6) is measured in seconds, the offset (C7) in μm , and the time (C7) to execute the commands in seconds.

Convergence Testing for Slice Resolution of Image Capture

The goal of this convergence testing was to identify the minimum slice resolution needed to accurately measure membrane height without compromising the efficiency of the system. The slice resolution refers to the distance traveled between each image captured. The team determined that a realistic range for slice resolution would be from 0.2 μm to 2 μm , the smallest increment possible with the stepper motor and the smallest increment possible with the microscope dial respectively. The following experiments were carried out by testing all available slice resolution values (0.2 μm , 0.4 μm , 0.6 μm , 0.8 μm , 1 μm , and 2 μm) on five membranes with the characteristics and naming conventions provided in Table 8. Each membrane is labeled with a number and letter corresponding to its location on the sample holder, followed by a unique number given to each sample holder, see Figure 31.

Table 8: Membrane Shape Configuration

Membrane Name	Membrane Surface Condition
1a - 10.5.4	Continuous Surface
11b - 10.3.2.2	Continuous Surface
14a - 6.5.4.2	Continuous Surface
9b - 10.3.3.1	Ruptured at Edge
14b - 10.7.3.2	Shallow Surface

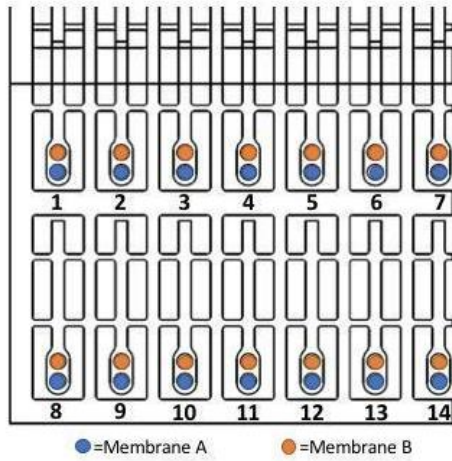


Figure 31: Membrane Naming Convention in Sample Holder

For each membrane sample, images were captured over a total Z height of 60 μm for all the available slice resolutions. The control variables for this test setup included a cell radius of 20 pixels and a cell pitch of 30 pixels.

Convergence Testing for Cell Radius and Cell Pitch of Image Processing

Cell radius and cell pitch are parameters used in the image processing script to make the analysis of individual images more efficient. A cell is a group of pixels averaged together to form a larger pixel. This method decreases image processing time by decreasing the number of pixels processed. The size of each cell is characterized by the radius and pitch, as previously illustrated in Figure 22. Consequently, these parameters affect the amount of detail in the generated plots. The effect of cell radius is illustrated in Figure 32 while the effect of a change in cell pitch is seen in Figure 33.

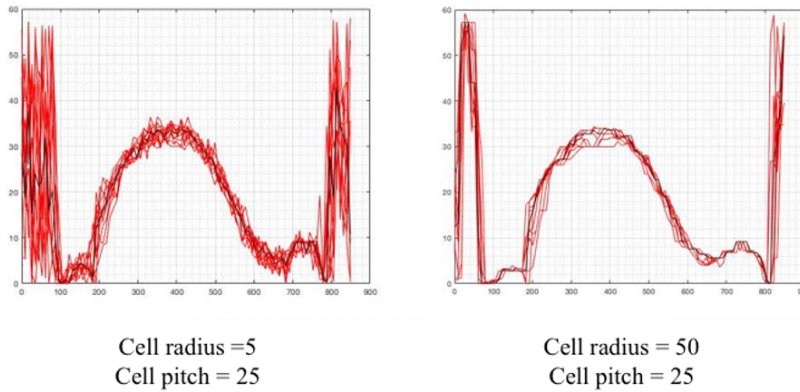


Figure 32: Effects of Cell Radius on 2D Plots

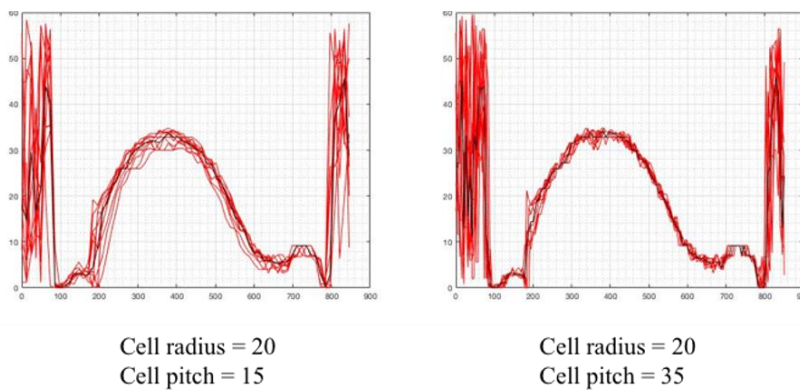


Figure 33: Effects of Cell Pitch on 2D Plots

The goal of convergence testing for cell radius and pitch was to find the appropriate proportions while considering the processing time. A total of three experiments were utilized to provide a range of optimal settings. These experiments were replicated for varying parameters of cell radius and cell pitch. The constants and variables of each test are described below.

Test 1: *Constant Cell Pitch = 25 pixels*

Varied cell radius from 5 to 50 pixels at increments of 5 pixels.

Test 2: *Constant Cell Radius = 30 pixels*

Varied cell pitch from 20 to 40 pixels at increments of 5 pixels.

Test 3: *Constant Cell Radius = 20 pixels*

Varied cell pitch from 15 to 35 pixels at increments of 5 pixels.

For all test combinations, five sets of 150 images at a slice resolution of $0.4 \mu\text{m}$ were analyzed through the image processing script to measure the height of the membrane. These five sets of images are from the five membrane samples listed in Table 8. For each test, to compare measurements between the five membrane samples, each measured height was normalized to the average height measured for that membrane.

3.4 Summary of Methodology

All methodology testing and investigations worked toward the goal of fully automating the optical inspection procedure of the hydrophone sensor membranes. The prototypes of the X, Y, and Z Axes of the microscope enabled further investigation into the capabilities of the image capture and processing systems. The complete system was then optimized to create an automated image capture process. The optimization testing provided evidence for the characterization of the control system for uniform optical inspection of hydrophone membranes. Once the team was able to understand the control system and the output measurements, the MATLAB scripts were optimized and debugged to increase user friendliness. The image capture and image processing scripts were needed to investigate the hardware and software capabilities that could be optimized. From the completion of an optimized image capture and processing procedure, a user manual was developed for the complete automated optical inspection procedure.

Chapter 4: Results and Discussion

The following chapter details the results from the methods explained in Chapter 3. This includes investigations regarding potential areas of error, control system characterization, and optimization of processing variables. Each section is detailed by the type of investigation along with findings and discussions to explain the data collected.

4.1 Potential Error Investigation Results

To optimize the Z-Axis system, the team reduced the observed areas of potential error previously described in Section 3.3.1.

To address the issue of vibrations transferring from the motor to the microscope, vibration isolating material was added to the base of the Z-Axis prototype. Additionally, this helps to stabilize the system because of the material's semi-adhesive property. To minimize the possible slip between the belt and pulley of the control system, the chosen belt includes compatible teeth on the side that has contact with the pulleys. To account for floating wires, connections without proper electrical communication, all wire connections were soldered and reinforced with heat-shrink tubing. A compounding source of error is the possibility for disconnected or misplaced wires from improper system setup and storage. To minimize the possibility of any system wiring disruptions, the team developed housing components for consistent storage and setup of all electrical components. To mediate the issue of providing an intermittent voltage supply to the motor, a 15V wall power supply with constant voltage output was implemented.

To complete the potential error investigation the offset of the motor was measured by testing its ability to move and return to its original position to evaluate motor performance. The test was replicated three times for each of the following slice resolutions: 0.2, 0.4, 0.6, 0.8, 1, and 2 μm . Table 9 shows the average stage offset calculated for each slice resolution along with the upper and lower limits of the 1 μm tolerance of the measuring device (Mahr Mechanical Dial Comparator, n.d.). The total calculated stage offset is $0.6 \mu\text{m} \pm 1 \mu\text{m}$, averaged from the 18 test results. Specific measurements for each slice resolution test run can be seen in Appendix D.

Table 9: Average Stage Offset and Micrometer Tolerance Added

Slice Resolution	Unit Size	Average Offset	Upper Tolerance	Lower Tolerance
0.2 μm	10 motor steps	1 μm	2 μm	0 μm
0.4 μm	5 motor steps	1 μm	2 μm	0 μm
0.6 μm	4 motor steps	0.3 μm	1.3 μm	-0.7 μm
0.8 μm	3 motor steps	0 μm	1 μm	-1 μm
1 μm	2 motor steps	0.3 μm	1.3 μm	-0.7 μm
2 μm	1 motor step	0.7 μm	1.7 μm	-0.3 μm

The results from Table 9 are shown with tolerance bars of $\pm 1 \mu\text{m}$ to include the measuring device tolerance, see Figure 34. The full findings of the tests can be found in Appendix D.

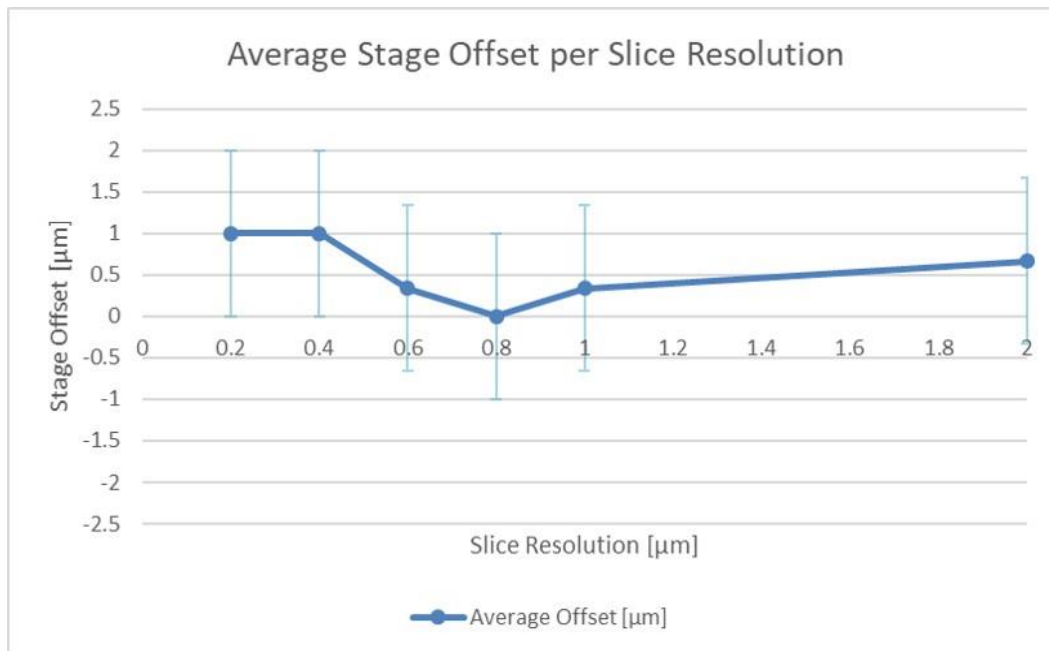


Figure 34: Average Stage Offset per Slice Resolution

The offset of the motor is considered during measurement collection because it is expected to compound if the control system is run in multiple membrane inspections, as it would during complete automation. This means the calculated offset of $0.6 \mu\text{m} \pm 1 \mu\text{m}$ must be factored into measurements as a tolerance.

4.2 Control System Characterization

The results of control system characterization testing provided insight into its capabilities. This allowed the team to present a realistic standard procedure for optical inspection that follows system functionality guidelines.

4.2.1 Magnification Level Investigation

The differences between the available magnification settings are depicted in Figure 35, which includes a sample image captured at each magnification setting of 5x, 10x, and 20x. With the standardization of the magnification level, consistent data collection and reliable image capture of the entire membrane shape can be obtained. This was not previously controlled in the fully manual procedure. The 10x magnification setting was chosen as the standard setting for all subsequent image capture with the objective of characterizing one membrane with the most representative and detailed data. At this setting, the image includes the whole membrane, unlike the 20x magnification, with higher resolution and detail than the 5x setting.

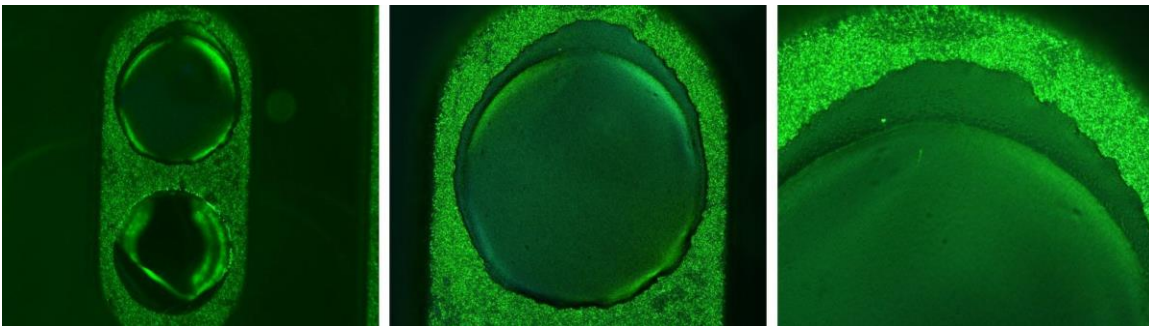


Figure 35: Membrane Sample at 5x, 10x, and 20x Magnification (left to right)

4.2.2 Pixel Size Calculations

The width and height of a standard captured image (2452x2056 pixels) is 840 μm and 700 μm respectively based on the calibration ruler, see Figure 36. These measurements equate 1 pixel to 2.9 μm . This value was applied within the MATLAB script to provide accurate measurements of the membrane in terms of micrometers. The pixel calibration value has a significant influence on the membrane characteristic measurements and is now a set parameter within the MATLAB processing script.

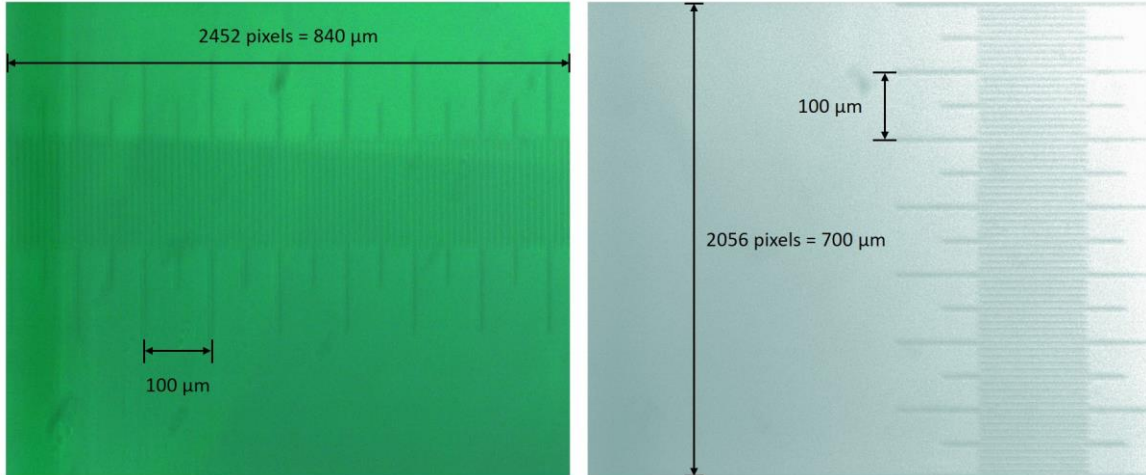


Figure 36: Calibration Ruler Measurements of Width (left) and Height (right), each tick is 10 μm

4.2.3 Z-Axis Dial Calibration

This section illustrates the results of both the manual and automated dial calibration which were used to ensure the motor produced accurate distances for the linear stage travel from the inputs of the MATLAB script.

Manual Calibration

The experimental values from the manual calibration provided the verification that one increment on the dial translates to slightly under 2 μm of linear stage distance in the Z direction. This confirms the statement in the microscope manual that one division of the focusing dial produces a vertical movement of approximately 2 μm (Leica, 1999, p.57). A summary of the results from the manual calibration for the Z-Axis dial is presented in Table 10 and the data can be found in Appendix E.

Table 10: Average Distance per Focusing Dial Increment

Operator	Average Distance (μm)
Sarah	1.89
Angela	1.88

Automated Calibration

Prior to developing the MATLAB scripts with specified distances for automated movements, the mathematical relationship between movement of the motor and microscope stage was calculated with three ratios. The manual calibration determined the ratio between stepper motor steps and linear distance of the stage (Ratio A) as 1 dial increment to 2 μm of linear distance of the stage. Ratio B is the compounded ratio of the “Stepper Motor to Pulley”

and the “Stepper Motor to Dial Increments (Non-Compounded)”, because the stepper motor does not directly mount to the dial. The automated calibration related stepper motor steps directly to dial increments (Ratio C) through the addition of Ratios A and B.

Ratio A = Dial Increments : Linear Distance of the Stage

Ratio B = Stepper Motor Steps : Dial Increments

Ratio C = Ratio A + Ratio B = Stepper Motor Steps : Linear Stage Distance

The calculation for Ratio B is described below to determine the compounded ratio between the motor and dial.

Stepper Motor to Pulley:

The ratio between the driving pulley on the rotating shaft of the stepper motor and driven pulley mounted to the focusing dial is 1:5.

$$\begin{aligned} &19 \text{ stepper motor driving pulley teeth} : 90 \text{ driven pulley teeth} \\ &1 : 5 \end{aligned}$$

Stepper Motor to Dial Increments (Non-Compounded):

The specification of the motor is that one step is 1.8° (Makeblock 81042, n.d.). One dial increment is a rotation of 3.6°. The ratio is 1:2 as one dial increment is equal to two stepper motor steps.

$$\begin{aligned} &1 \text{ stepper motor step} / 1.8^\circ \\ &100 \text{ dial incrementers} / 360^\circ = 1 \text{ dial increment} / 3.6^\circ \\ &1 : 2 \end{aligned}$$

Stepper Motor to Dial Increments (Compounded):

The “Stepper Motor to Pulley” and “Stepper Motor to Dial Increments (Non-Compounded)” ratios compound (Ratio C), because the motor does not directly connect to the dial.

$$10 \text{ stepper motor steps} = 1 \text{ dial increment}$$

Ratio C is calculated by relating Ratios A and B. This determines 1 stepper motor step to be equivalent to 0.2 μm of linear stage distance.

$$1 \text{ stepper motor step} = 0.2 \mu\text{m linear stage distance}$$

The final relationship of 1 stepper motor step to 0.2 μm of linear stage distance was then applied within the image capture MATLAB script to test if the mathematical calculations would remain valid for the control system operation. This was done by measuring the thickness of a titanium layer using the stepper motor. The testing results of this investigation are summarized in Table 11, with an average titanium layer thickness of 99.86 μm . The standard deviation of the 10 measurements is $\pm 0.8 \mu\text{m}$. This was compounded with the average microscope stage offset of $\pm 1.6 \mu\text{m}$, previously determined from the Potential Error Investigation (Section 4.1). The resultant tolerance of the automated calibration testing is a total of $\pm 2.4 \mu\text{m}$.

Table 11: Measured Titanium Layer Thickness

Test	Total Distance Measured (μm)
1	99.4
2	101
3	99.4
4	100
5	99.4
6	100.6
7	99.6
8	99
9	99
10	101.2
Average (μm)	99.86
Tolerance (μm)	± 2.4

The culmination of the dial calibrations provided evidence for the application of the final ratio result, 1 motor step to 0.2 μm , within the image capture process of the optical inspection procedure. This is because the average measured distance with the compounded tolerance includes the value of 100 micrometers, the expected measurement for the manufactured thickness of the titanium layer (ATI Flat Rolled Products, 2015).

The Z-Axis dial calibration provided the basis of all further testing setups. The culmination of the dial calibration results provided evidence for the application of the designed control system as the standard method for data collection of the optical inspection procedure. Quantifying and calibrating the relationship between the linear distance traveled to the rotation

of the stepper motor is integral to the function of the image capture and processing procedures. This is because it is the smallest slice resolution achievable with the stepper motor.

4.2.4 X and Y Axis Preliminary Dial Calibration

Preliminary testing was completed to relate X and Y motor steps to the stage movements in the X and Y directions. These movements are needed to transverse the sample holder to automatically inspect multiple membranes. This was done by centering and aligning the first membrane in view of the camera, inputting a number of steps into the programming software, and totaling the number of steps it takes for the next membrane to be centered in the camera frame.

The results from this testing are shown in Figure 37 along with the path used during testing for spacing values.

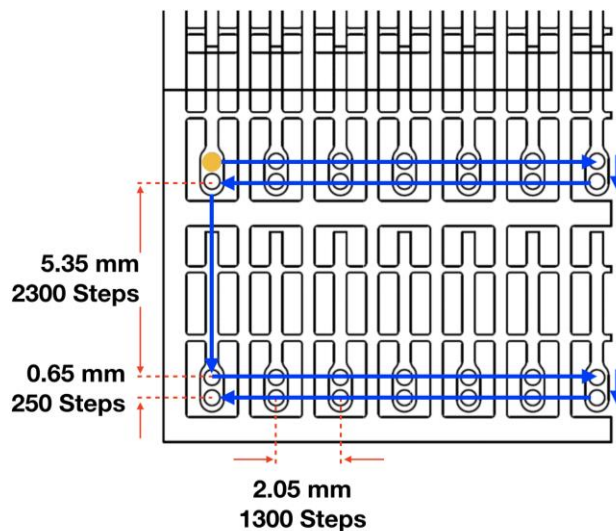


Figure 37: Configuration Tested for Preliminary X and Y Axis Control Investigation

The motors complete one revolution in 4096 steps (Schrittmotor, n.d.). This allows for finer motion control while still using full steps. With a reference frame of the front left corner of the microscope stage, the counter clockwise rotation of the X and Y dials move the microscope stage in the positive X and Y directions respectively. The sample holder must be in the orientation shown in Figure 37 or rotated 180°. If it were to be placed at 90° from this position, the investigated unit of steps between each membrane would no longer be valid. This is because the rotational motion from the X and Y dials does not translate to the same linear distance of stage travel.

The researchers now have a basis for further calibrating the X and Y dials for the complete automated inspection of a membrane sample holder to further reduce manual involvement in the optical inspection test. This investigation into X and Y motor movements ensured that the membrane is always within the camera frame and error in movements is not

compounded, such that the target is no longer in frame after multiple movements. The testing results provided in Figure 37 are based on preliminary investigations and should be verified through multiple iterations to refine the accuracy of the X and Y motor movements.

4.2.5 Measurement Parameters

For three membrane samples, height and diameter were calculated at three different cross-sectional areas to understand which measurement is the most consistent value for characterizing a membrane. Each membrane was analyzed at a cross section of no rotation, 10° rotation, and 90° rotation. This was done to observe the effects of rotation in theta on the 2D plots, mimicking different orientations of sample holder placement on the microscope stage. The 2D plots shown in Figures 38, 39 and 40 are the result of the different cross sections tested for one membrane sample as described in Section 3.3.2. The heights and diameters were calculated using three data cursor points. The results show that the alignment of the membrane influences the diameter measured more than the height measured.

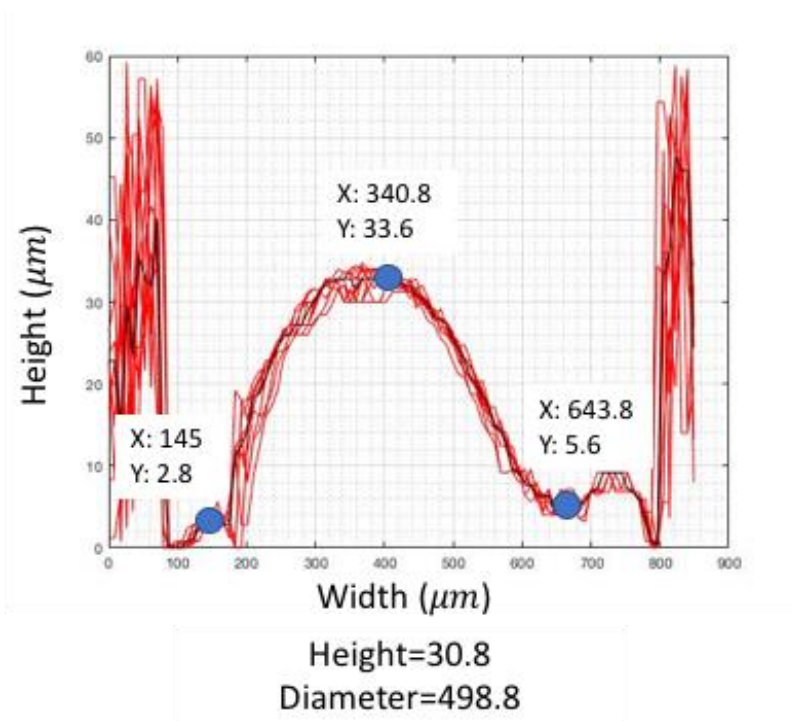


Figure 38: No Rotation - Membrane 1a

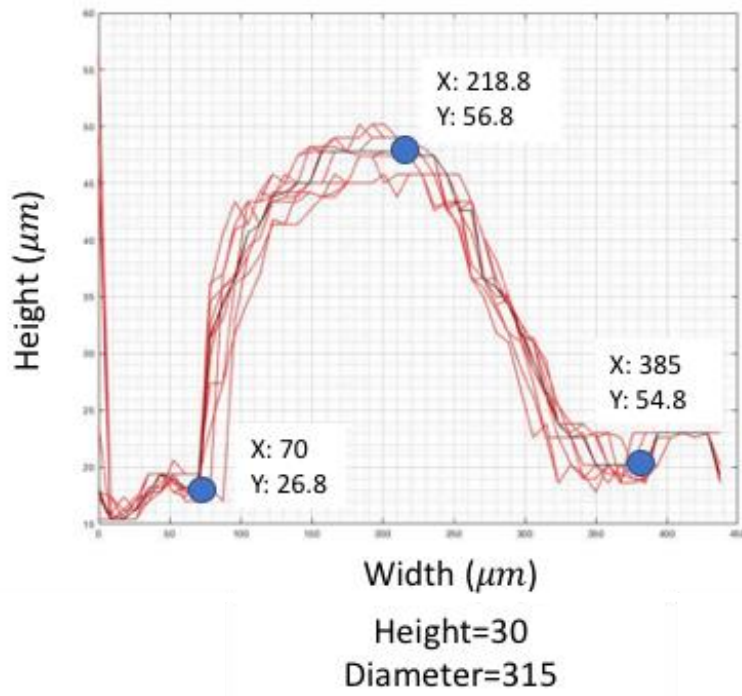


Figure 39: 10° Rotation - Membrane 1a

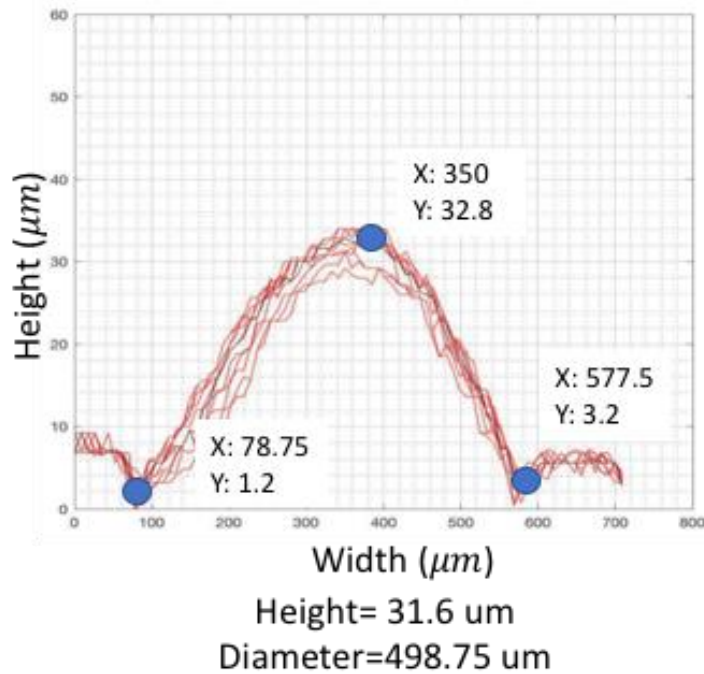


Figure 40: 90° Rotation - Membrane 1a

The results from Figures 38 and 39 illustrate a difference in diameter, 498.8 μm and 315 μm respectively. This difference is most likely related to the manual and nonuniform deposition of the membranes which creates discrepancies in membrane shape during manufacturing. As a result, the diameter changes at an inconsistent slope along the surface of the membrane. This is highlighted during the post-processing calculations by inconsistent measurements of diameter when analyzing different cross sections of the membrane shape.

Over the three post processing configurations of non-rotated, 10° rotation, and 90° rotation, height remained more constant than diameter as the cross-sectional area was changed for the given sample. The testing results from three membrane samples are seen in Table 12.

Table 12: Height and Diameter Measurements

	Membrane 1a		Membrane 14a		Membrane 11b	
Rotation	Height	Diameter	Height	Diameter	Height	Diameter
0°	30.8 μm	498.8 μm	26.4 μm	456.7 μm	46.8 μm	391.5 μm
10°	30.0 μm	315.0 μm	53.2 μm	369.7 μm	48.4 μm	224.7 μm
90°	31.6 μm	498.8 μm	22.4 μm	290.0 μm	50.0 μm	406.0 μm
Std. Dev.	0.8	106.1	16.7	83.4	1.6	100.7

The results for height measurement of Membrane 14a were less consistent than the measurements for Membranes 1a and 11b. The outlier is the measured height for 10° rotation. The hypothesis is the membrane has a larger height at this orientation, represented by the darker area circled in Figure 41. This area is considered for the 10° rotation, but not for the 0° or 90° rotation. The hypothesis is supported by the measured height from the 2D plots. An image of Membrane 14a for reference is seen in Figure 41.

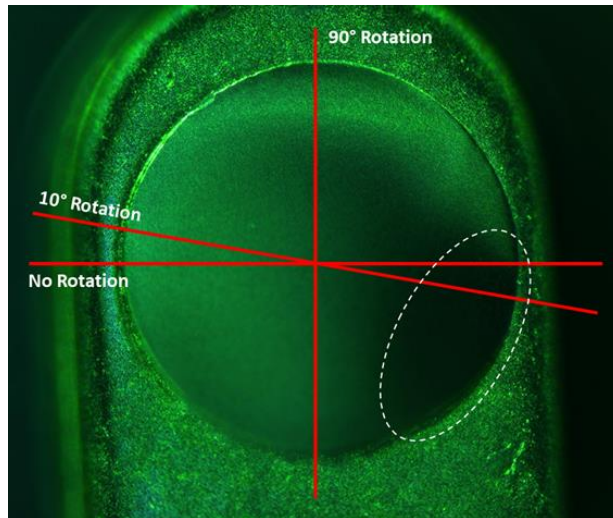


Figure 41: Membrane 14a

From this investigation the team decided to use the non-rotated cross-sectional area for all subsequent testing and analysis. Additionally, all membranes in the same sample holder will be measured in the same orientation on the microscope stage to be able to compare the results.

The 2D cross sections used for image analysis and quantitative membrane comparison were sufficient to measure height, but not diameter. This is due to inconsistent shape of the diameter throughout the height of the membrane. For this reason, the team determined the current image processing method is capable of providing more consistent height measurements than diameter measurements for a given membrane sample. Other processing methods should be researched to obtain diameter measurements to analyze and compare membranes.

4.3 Optimization Testing Results

The results of optimization testing provided evidence regarding the effects of changing the input variables during image capture and image processing.

4.3.1 Design of Experiments for Image Capture Presets

The team used Minitab 18 to generate a Pareto plot, based on the measured offset of the microscope stage, which illustrates the factors or combinations of factors that have a statistically significant influence on the measurement offset. For example, the Pareto chart in Figure 42 is calculated for a significance factor of 5% and corresponds to the DOE setup in Table 7. Neither the individual factors nor the combination of the two factors tested affect the offset measurement at a statistically significant level because they do not cross the red significance line. This was the same result for all slice resolutions tested (Appendix F).

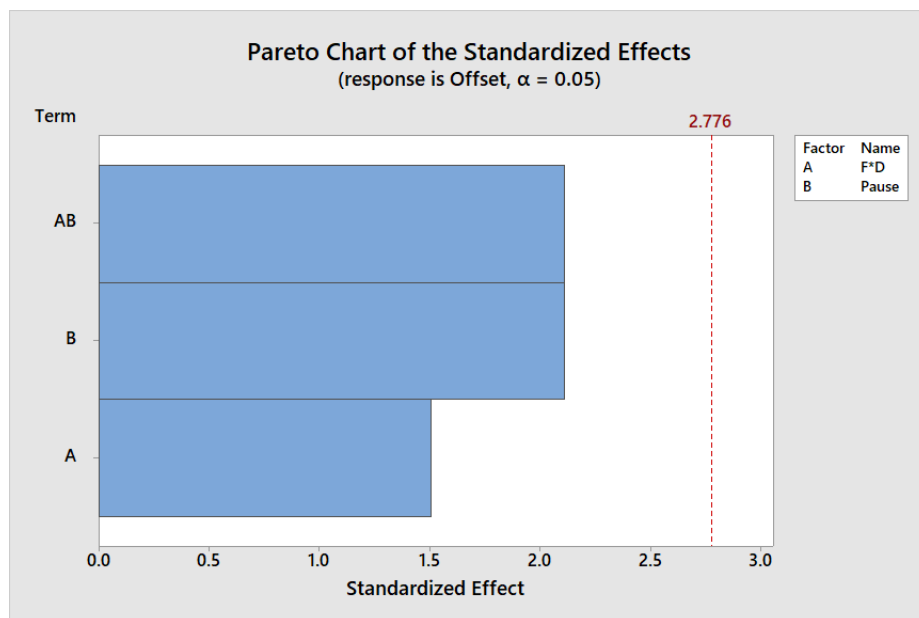


Figure 42: Example Pareto Chart of the Standardized Effects

The Main Effects and Interactions plots were utilized to understand the possible variation of test results. The Main Effects plot in Figure 43 displays the means for each value within a given factor. It also plots a reference line of the overall mean. With the factors having no significant influence on the offset measurement, this plot was used to visualize the maximum and minimum mean offset seen during testing of each frequency and duration combination.

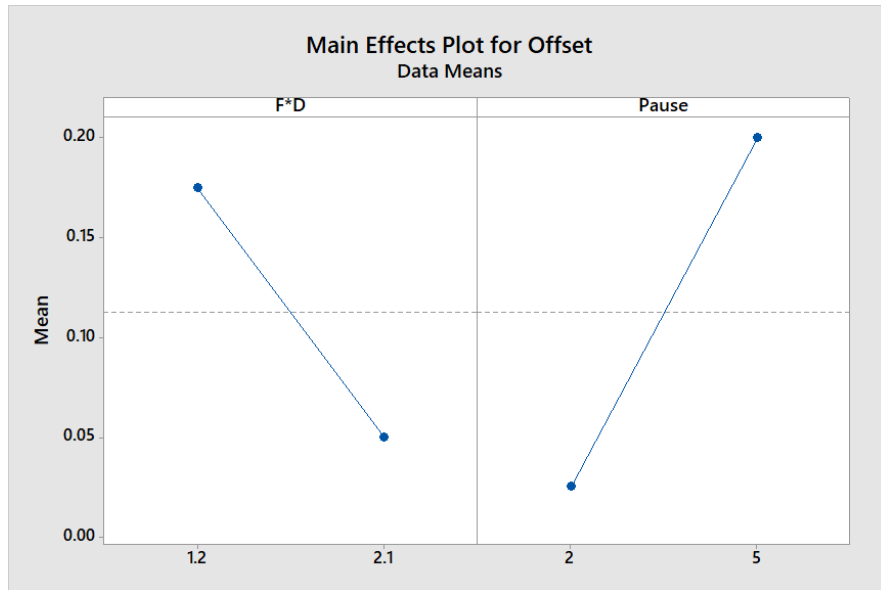


Figure 43: Main Effects Plot of Frequency, Duration and Pause

The Interactions Chart shows how the relationship between the response of one factor depends on the second factor, see Figure 44. This illustrated the largest mean offset found during testing to show the range of variation of all results.

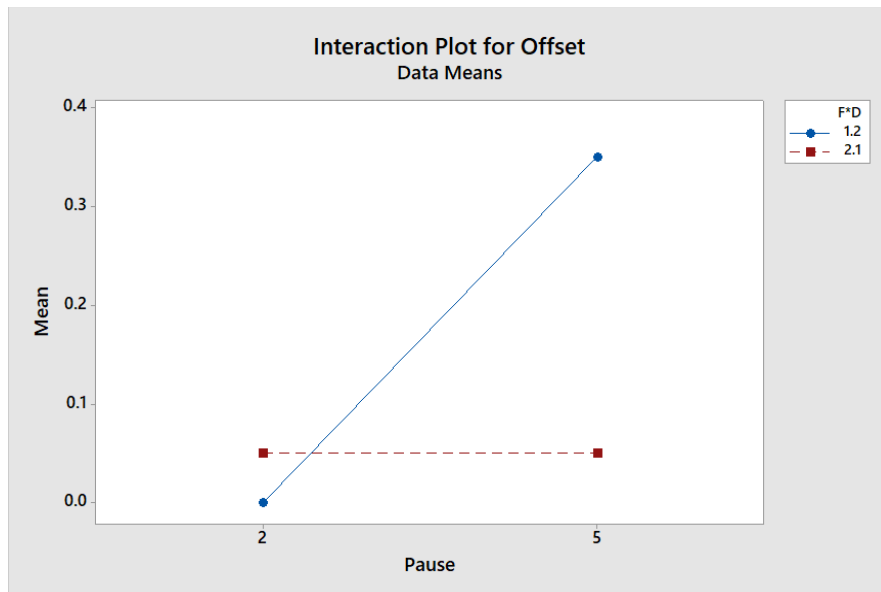


Figure 44: Interaction Plot of Frequency, Duration, and Pause

This led to the parameter groupings in Table 13 which ensure that acceleration from the motor will not affect performance and the overall image capture process can be executed efficiently. These groupings are applied within the MATLAB script for image capture dependent on the desired slice resolution. For instance, if an input of 0.8 μm is given as the slice resolution for image capture, the MATLAB script will call the values of 1 and 4 for frequency and duration, respectively. The recommended parameter groupings also allow for customizability of the system. For example, if a researcher only needs to complete a coarse scan of a membrane they can use a slice resolution of 2 μm .

Table 13: Configuration for Frequency/Duration and Pauses

Unit	Slice Resolution	Frequency (Hz)	Duration (sec)	Pause (sec)
10 motor steps	2 μm	2	5	2
5 motor steps	1 μm	5	1	2
4 motor steps	0.8 μm	1	4	2
3 motor steps	0.6 μm	3	1	2
2 motor steps	0.4 μm	2	1	2
1 motor step	0.2 μm	1	1	2

4.3.2 Convergence Testing for Slice Resolution of Image Capture

Through convergence testing, the minimum slice resolution value needed to accurately measure membrane height was identified. Five membranes were tested for all slice resolution values (0.2 μm , 0.4 μm , 0.6 μm , 0.8 μm , 1 μm , and 2 μm) to obtain a corresponding image set. All image sets were processed to measure the height of the membranes.

The measured height from the image processing script plots for each slice resolution was normalized as a percentage of the accepted value, the height measured for the smallest available slice resolution, 0.2 μm . This was chosen as the accepted value, because it is the highest plot resolution that can be achieved with the stepper motor. This testing allowed the team to see which lesser resolution provides data comparable to the highest resolution. This provides evidence for the conclusion regarding the necessary number of images to have a representative output yet efficient inspection process. Figure 45 illustrates the normalized height calculations and Table 14 lists the data points for the plot, standard deviations, and time to process each slice resolution. The standard deviation was calculated from the experimental error of data points at each slice resolution. This is plotted as the upper and lower limit boundaries in Figure 45 in red and yellow respectively. Data points not within these boundaries do not fall within the standard deviation. These boundaries statistically include 95% of all possible data sets for height

measurements to provide tolerance values for each slice resolution setting. The convergence data for the tolerance of diameter measurements can be found in Appendix G.

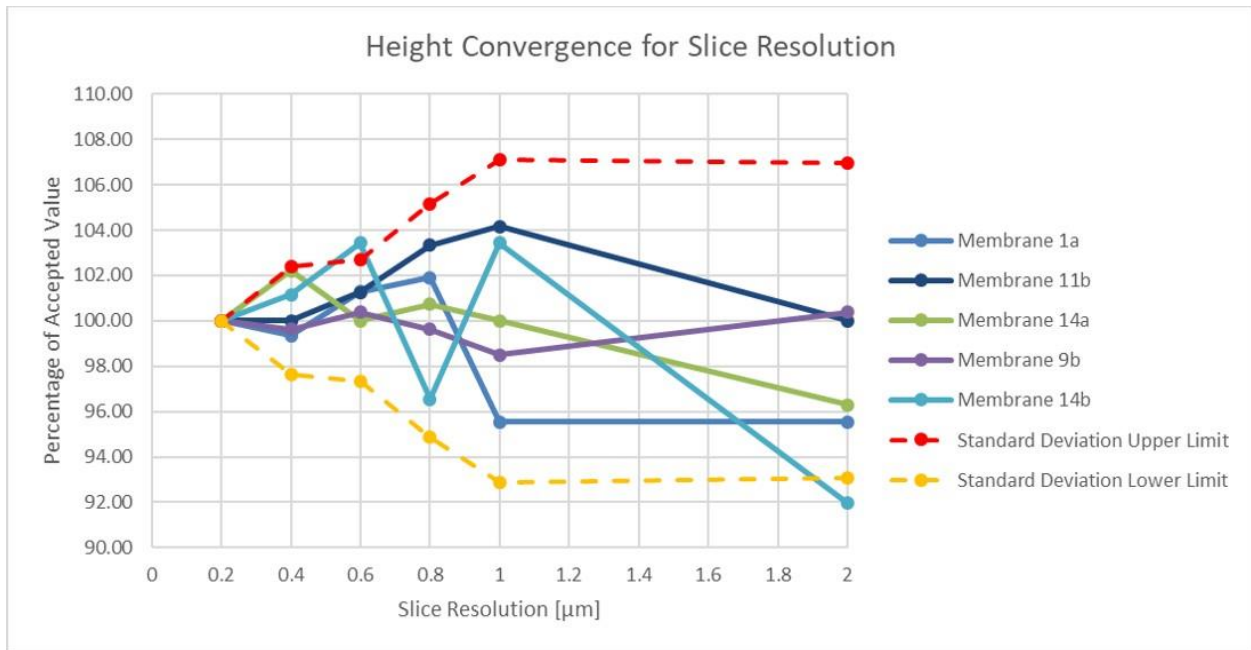


Figure 45: Height Convergence for Slice Resolution

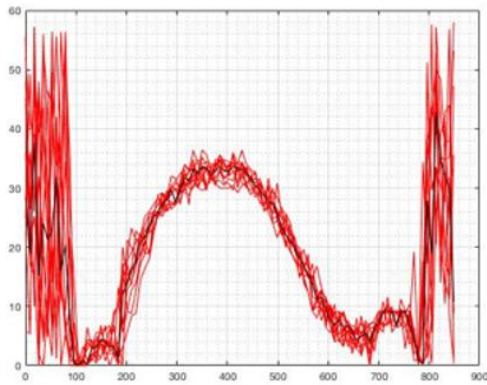
Table 14: Convergence Data Summary for Slice Resolution

No. of Images	Slice Resolution	± Std. Dev.	Average Image Processing Time
30	2 μm	7.0%	2.4 min
60	1 μm	7.1%	4.1 min
75	0.8 μm	5.1%	5.3 min
100	0.6 μm	2.7%	6.7 min
150	0.4 μm	2.4%	10.4 min
300*	0.2 μm	0%	21.8 min

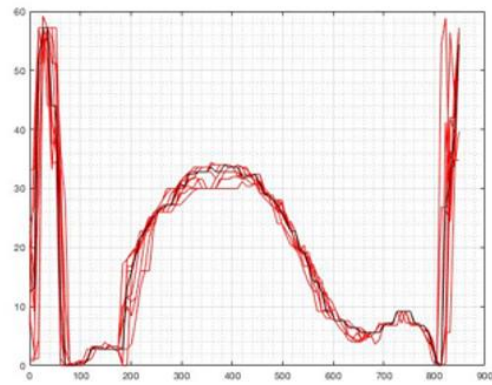
The team determined that the height measurements converge at 0.4 μm and 0.6 μm slice resolutions; 150 and 100 images over 60 μm respectively. The conservative slice resolution of 0.4 μm is an efficient processing input and is representative of the membrane shape. However, to add to the customizable design of the optical inspection procedure, Table 14 shows the tolerance for all tested slice resolutions if a shorter image capture and processing time is desired for membrane inspection.

4.3.4 Convergence Testing for Cell Radius and Cell Pitch of Image Processing

The team investigated the image processing parameters of cell radius and cell pitch to generate clear and representative models of membrane shape without compromising efficiency. The effects of changing cell radius and cell pitch are illustrated in Figures 46 and 47 respectively.

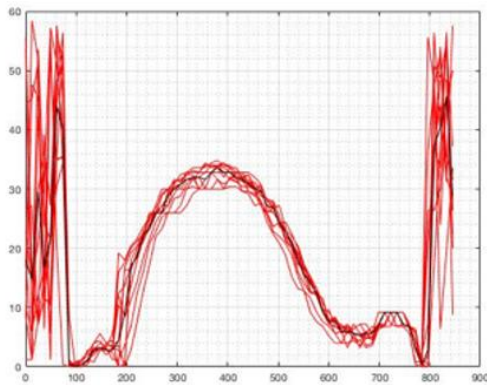


Cell radius = 5
Cell pitch = 25

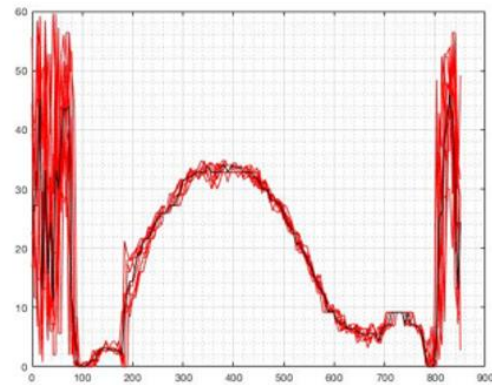


Cell radius = 50
Cell pitch = 25

Figure 46: Effects of Cell Radius on 2D Plots



Cell radius = 20
Cell pitch = 15



Cell radius = 20
Cell pitch = 35

Figure 47: Effects of Cell Pitch on 2D Plots

The following optimization experiments produced parameters to develop reliable and representative data with reduced interpolation between the focusing data of each captured image. The optimization of these parameters also provides researchers with a uniform method of quantifying membrane shape.

Figure 48 illustrates the height convergence values of cell radius with the control variable of 25 pixels for cell pitch from Test 1. From this plot it is observed that the least variance within the data is found between a cell radius of 25 to 35 pixels for the cell pitch of 25 pixels. For this cell radius range, the height measurements vary consistently, but have different processing times.

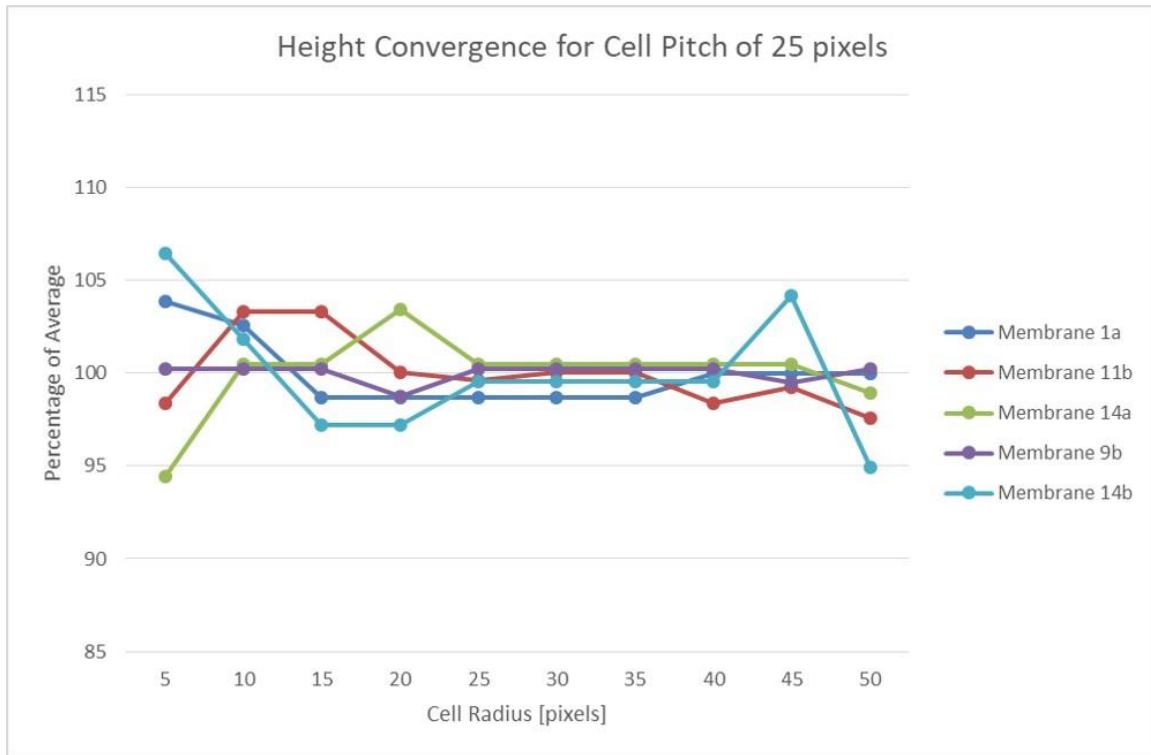


Figure 48: Height Convergence for Cell Pitch of 25 pixels

The combined results of Tests 1-3 provided three optimal post-processing parameter inputs for detailed plots and measurements with minimal processing time. The results from Tests 2 and 3 are found in Figures 49 and 50 respectively. Figure 49 displays the height convergence values of cell pitch with the control variable of 30 pixels for cell radius from Test 2. From the plot, the convergence value is seen between the cell pitch of 30 and 35 pixels, where the variation of normalized height measurements is the same across all tested membranes.

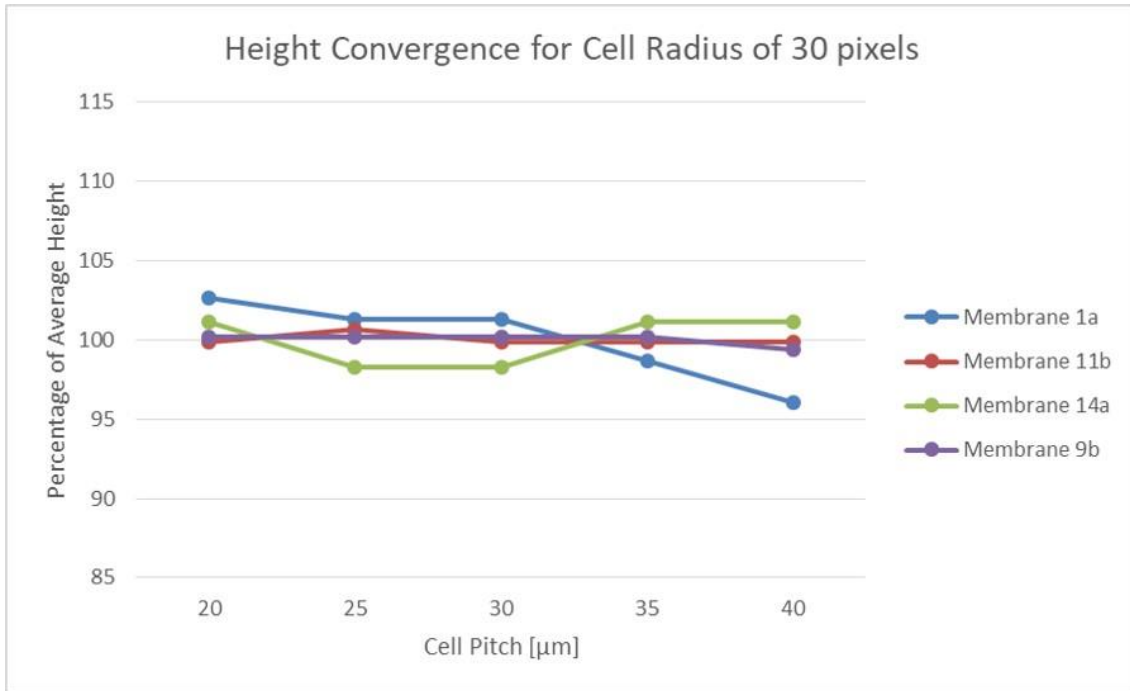


Figure 49: Height Convergence Plot with a Cell Radius of 30 pixels (Test 2)

Figure 50 displays the height convergence values of cell pitch with the control variable of 20 pixels for cell radius from Test 3. From the plot in Figure 50, the convergence value is taken where the variation in normalized height measurements is the smallest, at a cell pitch value of 20 pixels for a cell radius of 20 pixels.

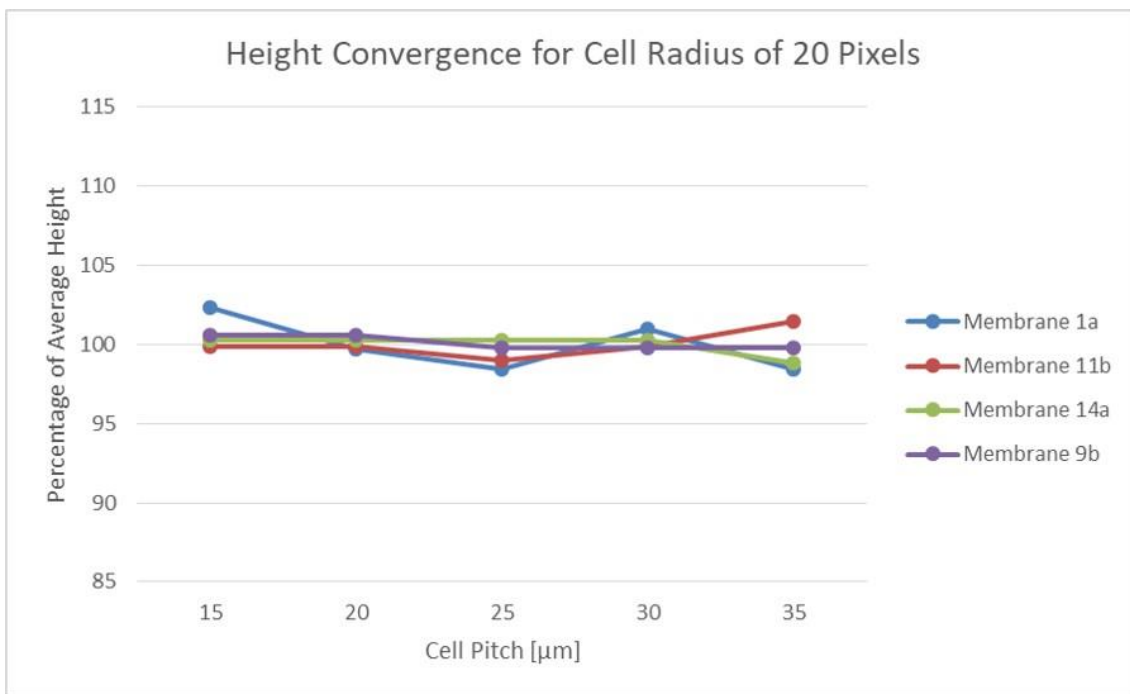


Figure 50: Height Convergence Plot with a Cell Radius of 20 pixels (Test 3)

The results from the convergence testing are summarized in Table 15. The average processing time pertains to the time it takes to analyze a set of 150 images in the image processing script when the cell radius and pitch are varied. The optimal cell radius and cell pitch configurations were chosen at points where all normalized data has similar variation. The convergence data for cell radius and cell pitch optimization testing can be found in Appendix H.

Table 15: Summary of Optimal Cell Radius and Cell Pitch Configurations

Cell Radius (pixels)	Cell Pitch (pixels)	Average Processing Time [min]
30	30, 35	5.25, 3.9
25	25	5
20	20	5.5

The results from the three tests for cell radius and pitch convergence led to the conclusion that the established parameters do not compromise the development of 2D and 3D models that accurately represent membrane shape.

Chapter 5: Conclusion

The Automated Optical Inspection of MEMS Based Cochlear Implant Hydrophones MQP provided the USZ research team with a functional Z-Axis control system and working X and Y Axis prototypes for the future fully automated optical inspection of hydrophone membranes. Previously, the manual optical inspection procedure took an average of 1 hour per membrane to capture and process 15 images. This manual procedure was too inefficient to be realistically implemented as a standard lab procedure and did not provide sufficient data to make conclusions about the membrane shape. Through research, prototyping, optimization, and analysis, the research team now has a feasible method of incorporating optical inspection into the membrane quality control process. The hardware designed for the optical inspection process is specific to the functions of the available microscope, yet is removable to use the equipment for other research purposes. The image processing capabilities have been optimized from a minimum slice resolution of $2\ \mu\text{m}$ to $0.2\ \mu\text{m}$ with minimized potential error within the control system setup at the 10x magnification level. This new automated procedure reduces membrane inspection to about 30 minutes to capture and process 150 images, including 10 minutes of manual involvement. After implementation, the research team will be able to quantitatively characterize membrane shape through the consistent calculation of height measurements to establish parameters for a functional membrane. A visual representation of the differences between the unstandardized procedure and standardized optimized procedure can be seen in Figure 51 and 52 respectively.

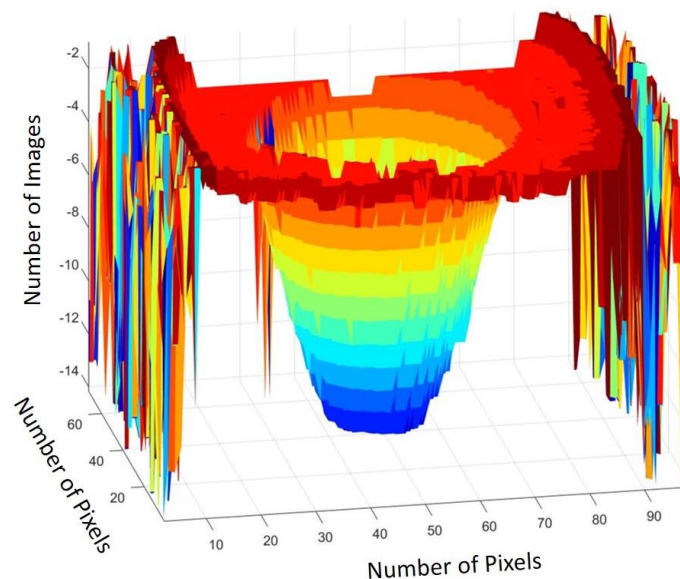


*Figure 51: Characterization of Hydrophone Sensor Membrane from August 14th
15 images, Slice Resolution of $4\ \mu\text{m}$, Total Image Capture (Manual) and Processing Time of 1 hour per Membrane*

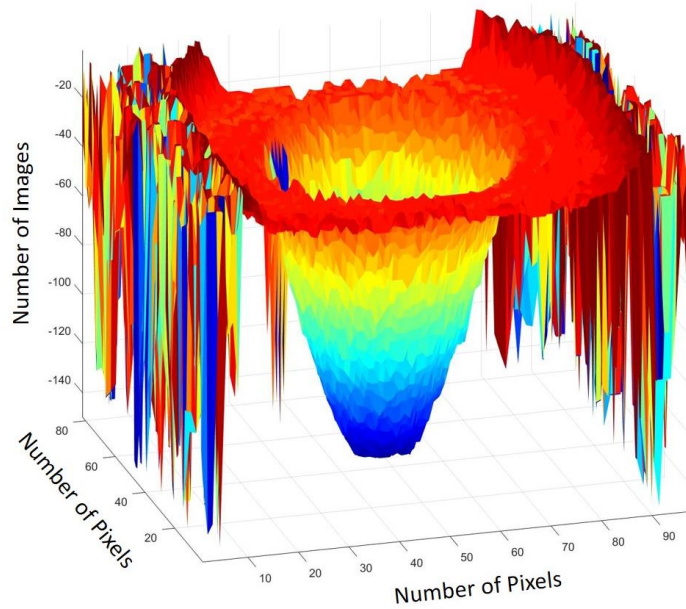


*Figure 52: Characterization of Hydrophone Sensor Membrane from October 5th
150 images, Slice Resolution of 0.4 μm , Total Image Capture (Automated) and Processing Time of 30 minutes per Membrane*

From the established optimized parameters of image capture settings, slice resolution, cell pitch and cell radius, the team created a User Manual (Appendix I) detailing a uniform image capture and post-processing procedure with customizable parameters and test setups available to the researchers. Customizability was an added factor due to the preliminary state of membrane optical inspection at USZ.

This provides the USZ research team with the opportunity to improve upon the automated system for a faster integration into standard lab procedures. The remaining sections present recommendations for further investigation and improvements of the Z-Axis optical inspection procedure and X and Y Axis controls for a fully automated system.

Chapter 6: Recommendations

This chapter includes all recommendations for further development of the control system for optical inspection. If implemented, the system will be fully automated and more helpful for the user.

6.1 Z-Axis Recommendations

To further optimize and refine the Z-axis image capture and characterization of hydrophone membranes, the team provides the following recommendations to the USZ research team:

- Add a pre-scan of each membrane being inspected to identify the top and bottom of the curvature for an accurate height span during data collection. This will shorten the height spanned by the image capture process, reducing the necessary number of images and expected completion time.
- Add buttons to the MATLAB script to control movements of the motor for a more user-friendly interface when focusing on the top titanium surface for the beginning of the image capture process. This will allow the user to leave the motor's power source on while positioning the specimen underneath the microscope lens, removing the risk of forgetting to power on the motor when beginning the image capture process.
- Improve the GUI through the addition of input fields for file directory and saving location. This will remove the risk of users forgetting to change a file directory for image capture and overriding previously captured images.
- Investigate the precision of the camera optics with the hydrophone membrane and titanium as targets for spatial resolution. This will provide testing results to understand at what increments the system can differentiate between features.
- Investigate additional parameters such as radius of curvature or standardizing the measuring points for the diameter of a membrane. This will provide researchers with more parameters to compare sample-to-sample data.
- A suggested method for measuring diameter would be to analyze each image by fitting a circle around the circumference of the focused membrane shape. Then, the processing script can stack these images to develop a 3D conical representation of the membrane. This would provide researchers with a comparable method of processing for diameter analysis.

6.2 X & Y Axis Recommendations

To incorporate motorized X and Y axis movements into a fully automated optical inspection system, the team provides the following recommendations to the USZ research team:

- Utilize the Arduino Library in MATLAB to investigate functions for controlling three motors from one Arduino. This will be the next step for developing a fully automated optical inspection procedure of one membrane sample holder.
- Calibrate the approximate distance traveled by one step of the motors used for the X & Y axis movement. This will help develop MATLAB functions for more accurate positioning of the membrane sample under the center of the microscope lens.
- Add programmable buttons to move the motors manually. When the stepper motors are connected to the X and Y dials (regardless if they are connected to a power source) the dials cannot be physically turned. This will enable the operator to use the calibrated distance of one motor step for precise positioning in the image capture window.
- Develop a standard holder to place the membranes in the same orientation under the microscope lens. This allows the samples to lay flat while in a precise horizontal position under the microscope lens for proper movement between membranes.

This automated optical inspection system is intended for the quality control process of hydrophone membranes, but the automated motor control of the microscope dials can be utilized for other optical inspection applications with specified focusing points.

References

- 42BYGHW6094P1 Stepper Motor (Makeblock 81042). (n.d). Retrieved from <https://rlx.sk/enstepper-mottor/2932-42byghw609d4p1-stepper-motor-makeblock-81042.html>
- ATI Flat Rolled Procuts. (2015). *Certificate of Conformance* (TI GR2 .004”X 16.937”). Pico Rivera, CA: Author.
- Automatic Optical Inspection, AOI systems. (n.d.). Retrieved August 16, 2018, from <https://www.electronics-notes.com/articles/test-methods/automatic-automated-test-ate/aoi-optical-inspection.php>
- Caddy (n.d.) Cushioned Pipe Clamp, Tube Size 1 In [Electronic]. Retrieved from <https://www.amazon.com/Cushioned-Pipe-Clamp-Tube-Size/dp/B000R8LF8Q>
- D. (2018, August 04). How To Control Stepper Motor with A4988 Driver and Arduino. Retrieved from <https://howtomechatronics.com/tutorials/arduino/how-to-control-stepper-motor-with-a4988-drvier-and-arduino/>
- Dobrev, Ivo (2018, August 14). Personal interview with Ivo Dobrev.
- DroneBot Workshop. (2018, March 20). Stepper Motors with Arduino. Retrieved from <https://dronebotworkshop.com/stepper-motors-with-arduino/>
- How Minitab stores design information in the worksheet. (2017). Retrieved October 2, 2018, from <https://support.minitab.com/en-us/minitab/18/help-and-how-to/modeling-statistics/doe/supporting-topics/basics/how-minitab-stores-design-information/>
- Keyes A4988 Stepper Driver Modul mit Breakout. (n.d.). Retrieved from <https://www.play-zone.ch/de/elektronik-kit-zubehoer/servos-motoren/motoren-treiber/keyes-a4988-stepper-driver-modul-mit-breakout.html>
- Leica. (1999). *Leica DMR: Instructions*. Wetzlar, Germany: Author.
- Mahr Mechanical Dial Comparator. (n.d.). *Millimess 1002(Z) - 1050(Z) Operating Instructions*. Retrieved from

<https://www.mahr.com/scripts/relocateFile.php?ContentID=190890&NodeID=22307&FileID=13274&ContentDataID=260563&save=0&isBlog=0>

Microscope Stages - Microscope Stage. (n.d.). Retrieved from <https://dovermotion.com/products/linear-stages/microscope-stages/>

National Institute on Deafness and Other Communication Disorders (NIDCD). (2017, March 6). *Cochlear Implants*. Retrieved from <https://www.nidcd.nih.gov/health/cochlear-implants>.

Pfiffner, F., Prochazka, L., Peus, D., Dobrev, I., Dalbert, A., Sim, J. H., . . . Huber, A. (2017). A MEMS Condenser Microphone-Based Intracochlear Acoustic Receiver. *IEEE Transactions on Biomedical Engineering*, 64(10), 2431-2438. doi:10.1109/tbme.2016.2640447

Process digital images with computer algorithms. (2018). In MathWorks. Retrieved from <https://www.mathworks.com/discovery/digital-image-processing.html>

Prochazka, Lukas (2018, August 15). Personal interview with Lukas Prochazka.

Schrittmotor / Stepper Motor 12V 1/64. (n.d.). Retrieved from <https://www.play-zone.ch/de/elektronik-kit-zubehoer/servos-motoren/stepper-schrittmotoren/schrittmotor-stepper-motor-12v-1-64.html>

Stepper Motor Basics. (n.d.). Retrieved from <https://www.orientalmotor.com/stepper-motors/technology/stepper-motor-basics.html>

UniversitätsSpital Zurich. (n.d.a). ICAR Sensor Overview – Generation 3 Image 1 [Photograph].

UniversitätsSpital Zurich. (n.d.b). ICAR Sensor Overview – Generation 3 Image 2 [Photograph].

Yip, M., Jin, R., Nakajima, H. H., Stankovic, K. M., & Chandrakasan, A. P. (2015). A fully-implantable cochlear implant SoC with piezoelectric middle-ear sensor and arbitrary waveform neural stimulation. *IEEE journal of solid-state circuits*, 50(1), 214-229. Retrieved from <https://ieeexplore.ieee.org/abstract/document/6910323/>

Appendix A: Interview with Dr. Lukas Prochazka for current manual process

Transcribed below is a summary of the topics discussed by Dr. Lukas Prochazka when asked to demonstrate the current manual optical inspection procedure. The image capturing software that is used prior to MATLAB processing is called ZEN.

Step 1: Setup

- a) Using the red switch on the power supply at the microscope station, turn on the mercury powered microscope light
- b) Open ZEN to ensure proper firewire camera connection

Step 2: Sample Preparation

- a) Clean off any dust which may be on the microscope stage with an air compressor
- b) While wearing gloves, pick up the sensor sample holder with tweezers and place on the microscope slide for inspection
- c) Using the X, Y, and Z axis focusing dials bring one membrane into view by focusing on the surface of the upper titanium layer (both 5x and 10x magnification have been used, but there is not a standard measurement)

Step 3: Image Capture

- a) After focusing the microscope on the upper layer of titanium, move the microscope stage down a few increments on the Z-axis focusing dial to ensure images are captured if the membrane is curved upward.
- b) Take one image using ZEN, then move the microscope stage upward one or two increments on the focusing dial.
- c) Take a second image and repeat the action of moving the microscope stage upward one or two increments on the focusing dial.
- d) Repeat the image capture process until you believe the entire membrane has been captured
- e) Save all images to a folder on the computer network for post processing

Step 4: MATLAB Post Processing

- a) Use the folder of images along with the MATLAB script named “MQP_2018_Shape_Scan” to stack the images and develop a 3D model of the membrane
- b) There is not a specific parameter the researchers look for when characterizing the membrane. Previously the researchers did not have a way to understand if static loading or acoustic loading tests have an effect on the shape of the membrane.

Prochazka, Lukas (2018, August 15). Personal interview with Lukas Prochazka.

Appendix B: Wiring of Z-Axis Control System

The wiring for the control system was based on the wiring found when researching example system control designs, such as the one shown in Figure 1. The two-phase stepper motor has two wires per coil, with a total of 4 wires to be connected to the 2B, 2A, 1A, and 1B pins of the A4988 driver. The specifications for the stepper motor provided the information about the phase of the wires and their pairings, shown in Table 1 below. The order can be switched as long as wires of opposite phases are kept together. The black and green wires in Table 1 can be either A and B and the red and blue wires can also be either A or B, but the wires of the same phase cannot both be A or B. Switching the pairings of the phases will change the default direction of the motor. Pins for step and direction of the motor need to be connected to Arduino pins that can be configured as digital outputs. The Arduino Mega 2560 has digital pins numbered from 22 to 53 and pulse width modulated (PWM) pins numbered from 2 to 13. All pins are available for use and must be identified and configured properly for step and direction when programming the system. The team decided to use a PWM pin for step as this sends and changes digital output faster for stepping. The direction pin was connected to a digital Arduino pin since there are fewer commands for direction. The power input requires a range of 8 to 35 volts, and the power supply is connected to the VMOT (motor voltage) and ground pins. The system also requires logic voltage that is provided by the Arduino controller which is connected to the VDD and grounds pins with a voltage range of 3 to 5.5 volts.

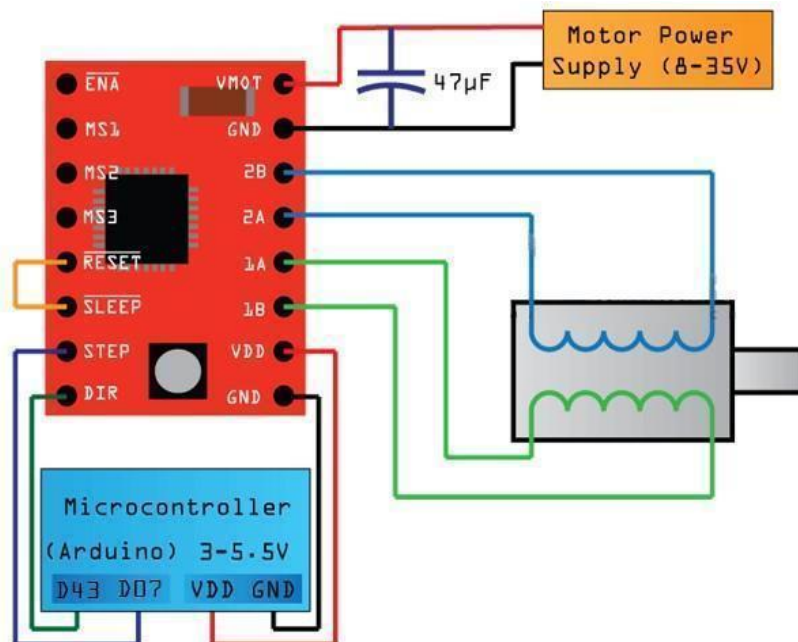


Figure 1: Control System Wiring (D. 2018, August 04)

Table 1: Phase and Driver Pin Configurations (Makeblock 81042, n.d.)

Wire Color	Phase	Driver Pin
Red	A+	2B
Black	A-	2A
Blue	B+	1B
Green	B-	1A

The breakout module seen in Figure 2 was used to integrate the wiring of the motor, driver, controller, and power sources. A breadboard could have been used for this purpose. However, this module makes the wiring more intuitive and ensures correct connections since the pins that need to be wired are labeled and exposed. The driver with two columns of 8 pins is placed in the center of the module and it also contains the required circuit components including a 100 μ F capacitor and two 472 μ Ohm resistors.

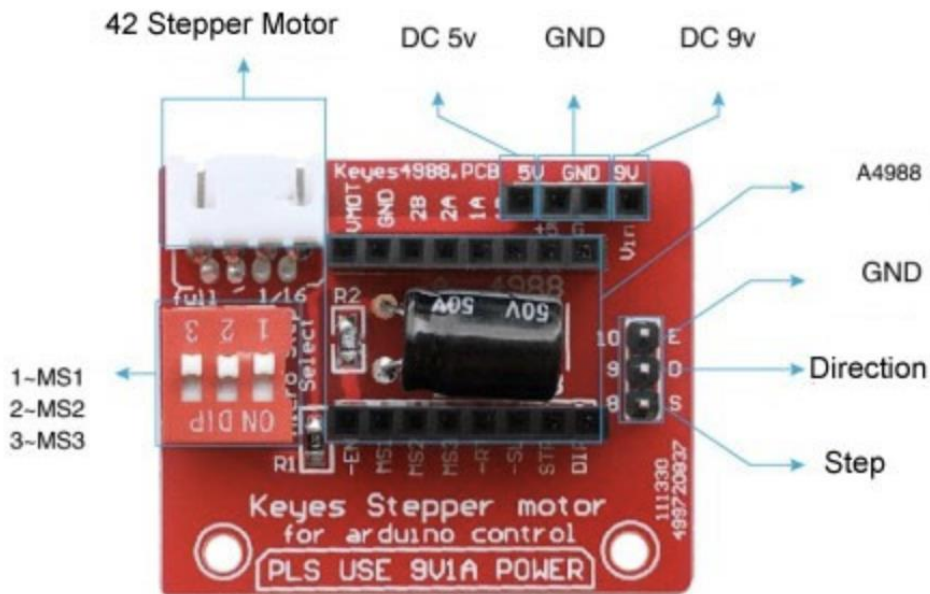


Figure 2: Keyes Stepper Motor Modules for Arduino Control (“Keyes A4988 Stepper Driver Module”, n.d.)

Appendix C: Wiring of X and Y Axis Control System

Figure 1 illustrates the basic wiring of the unipolar motors used to control the X and Y axis movements of the automated microscope. The motors have four pins to control step and direction, unlike the Z-Axis control with a total of two pins for motion control and programming. To incorporate one power source for both motors, a breadboard was used with a 9V power source. To program movements in MATLAB, the Arduino library must be used. The motors were controlled with the Arduino user interface for all preliminary investigation.

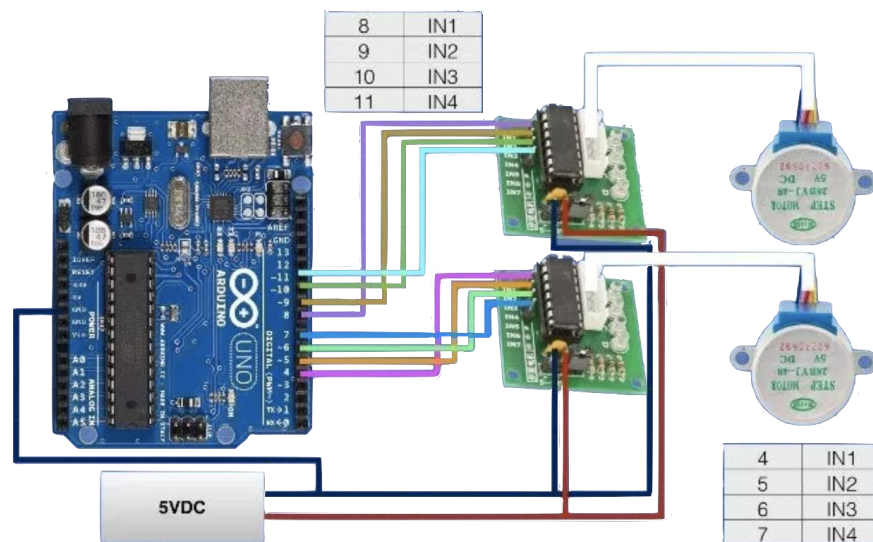


Figure 1: X and Y Axis Stepper Motor Wiring Diagram (DroneBot Workshop, 2018, March 20)

Appendix D: Stage Offset Testing

This experiment tested the ability of the motor to return to its original position during the image capture process. For these tests the starting and final position of the stage was measured with a Mahr Millimes 1003 micrometer with a tolerance of $\pm 1\mu\text{m}$ to measure the final stage offset in microns (Mahr Mechanical Dial Comparator, n.d.). These measurements were then used to characterize the performance of the motor.

Table 1: Stage Offset Measurements for all Slice Resolution Tests

Slice Res: 0.2 μm	150 steps = 30 μm	150 steps = 30 μm	150 steps = 30 μm	
	Loop = 150	Loop = 150	Loop = 150	
F.D = 1.1 (0.2 μm)	Measurement 1	Measurement 2	Measurement 3	
Start Value [μm]	-5	-8	-13	
End Value [μm]	-6	-9	-14	AVERAGE
Offset [μm]	1	1	1	1

Slice Res: 0.4 μm	150 steps = 30 μm	150 steps = 30 μm	150 steps = 30 μm	
	Loop = 75	Loop = 75	Loop = 75	
F.D = 2.1 (0.4 μm)	Measurement 1	Measurement 2	Measurement 3	
Start Value [μm]	-5	-11	-15	
End Value [μm]	-6	-12	-16	AVERAGE
Offset [μm]	1	1	1	1

Slice Res: 0.6 μm	150 steps = 30 μm	150 steps = 30 μm	150 steps = 30 μm	
	Loop = 50	Loop = 50	Loop = 50	
F.D = 3.1 (0.6 μm)	Measurement 1	Measurement 2	Measurement 3	
Start Value [μm]	-8	-13	-7	
End Value [μm]	-8	-13	-8	AVERAGE
Offset [μm]	0	0	1	0.3

Slice Res: 0.8 μm	160 steps = 32 μm	160 steps = 32 μm	160 steps = 32 μm	
	Loop = 40	Loop = 40	Loop = 40	
F.D = 1.4 (0.8 μm)	Measurement 1	Measurement 2	Measurement 3	
Start Value [μm]	-7	-7	-10	
End Value [μm]	-7	-7	-10	AVERAGE
Offset [μm]	0	0	0	0

Slice Res: 1 μm	150 steps = 30 μm	150 steps = 30 μm	150 steps = 30 μm	
	Loop = 30	Loop = 30	Loop = 30	
F.D = 5.1 (1 μm)	Measurement 1	Measurement 2	Measurement 3	
Start Value [μm]	-13	-5	-6	
End Value [μm]	-13	-6	-6	AVERAGE
Offset [μm]	0	1	0	0.3

Slice Res: 2 μm	150 steps = 30 μm	150 steps = 30 μm	150 steps = 30 μm	
	Loop = 15	Loop = 15	Loop = 15	
F.D = 2.5 (2 μm)	Measurement 1	Measurement 2	Measurement 3	
Start Value [μm]	-8	-17	-5	
End Value [μm]	-9	-18	-5	AVERAGE
Offset [μm]	1	1	0	0.7

Appendix E: Focusing Dial Calibration and 5x vs. 10x data results

The team confirmed the actual difference in measurement between the two surfaces where we “start” and “stop” the measurement is 0.1mm through an interview with Dr. Lukas Prochazka along with specifications provided by the manufacturing company. To calculate the value of each increment, the team utilized a formula ending with a measurement in μm . The formula used is as follows:

$$(\mu\text{m})/\text{increment} = (0.1 \text{ mm} / \# \text{ of increments moved}) * 1000$$

To reduce any operator to operator, influence on measurements, 2 operators were used for a set of measurements for both the 5x and 10x magnification. This resulted in a total of 4 measurements for the potential value of one increment on the focusing dial of the microscope. An example of test data for the 5x and 10x magnification can be seen in Tables 1 and 2 below, both from one operator. The final measurements for all 4 tests are summarized in Table 3. A key observation within the test data is that each starting measurement does not have the same value. This is because the operator of the test focused the sample by observation to ensure there would not be any bias within the data if the operator tried to hit the same increment value each trial.

Table 1: 5x Magnification Focusing Dial Calibration Measurement

Operator:	Sarah Bachli		5x Magnification	
Sample	Start Increment	Stop Increment	Increments Moved (Start – Stop)	Value of Each Increment (μm)
Trial 1	70	25	45	2.22
Trial 2	69	26	43	2.33
Trial 3	76	22	54	1.85
Sample 2	Start Increment	Stop Increment		
Trial 1	70	31	39	2.56
Trial 2	82	23	59	1.69
Trial 3	69	27	42	2.38
Sample 3	Start Increment	Stop Increment		
Trial 1	70	19	51	1.96
Trial 2	76	25	51	1.96
Trial 3	74	25	49	2.04
Sample 4	Start Increment	Stop Increment		

Trial 1	71	25	46	2.17
Trial 2	69	23	46	2.17
Trial 3	74	21	53	1.89
Sample 5	Start Increment	Stop Increment		
Trial 1	71	23	48	2.08
Trial 2	68	23	45	2.22
Trial 3	69	19	50	2.00
Average increment value (μm)=1.97 μm				

Table 2: 10x Magnification Focusing Dial Calibration Measurement

Operator:	Sarah Bachli	10x magnification		
Sample 1	Start Increment	Stop Increment	Increments Moved (Start – Stop)	Value of Each Increment (μm)
Trial 1	82	33	49	2.04
Trial 2	83	31	52	1.92
Trial 3	87	33	54	1.85
Sample 2	Start Increment	Stop Increment		
Trial 1	86	33	53	1.89
Trial 2	85	33	52	1.92
Trial 3	85	34	51	1.96
Sample 3	Start Increment	Stop Increment		
Trial 1	86	32	54	1.85
Trial 2	86	34	52	1.92
Trial 3	86	34	52	1.92
Sample 4	Start Increment	Stop Increment		
Trial 1	84	33	51	1.96
Trial 2	85	32	53	1.89
Trial 3	84	32	52	1.92
Sample 5	Start Increment	Stop Increment		
Trial 1	84	33	51	1.96
Trial 2	83	32	51	1.96
Trial 3	84	33	51	1.96

Average increment value (μm)=1.81

Table 3: Results for Average Increment Value of the Focusing Dial

Operator	Magnification	Average Increment Value (μm)
Sarah	5x	1.97
Sarah	10x	1.81
Angela	5x	1.97
Angela	10x	1.78

The two increment values found by each operator were averaged to provide the data in Table 3 of Section 4.

Appendix F: Design of Experiment Analysis for Image Capture Presets

The following Pareto Charts were developed using Minitab 18 based on the measured offset of the microscope stage, which illustrates the factors or combinations of factors that have a statistically significant influence on the measurement offset.

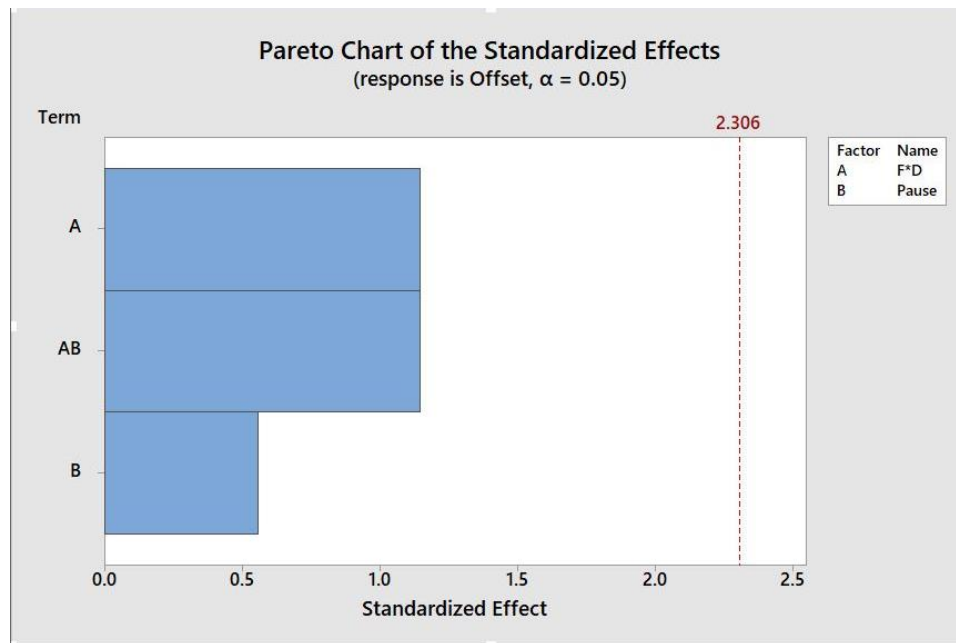


Figure 1: Pareto Chart for DOE of Slice Resolution 2 μm (30 Images)

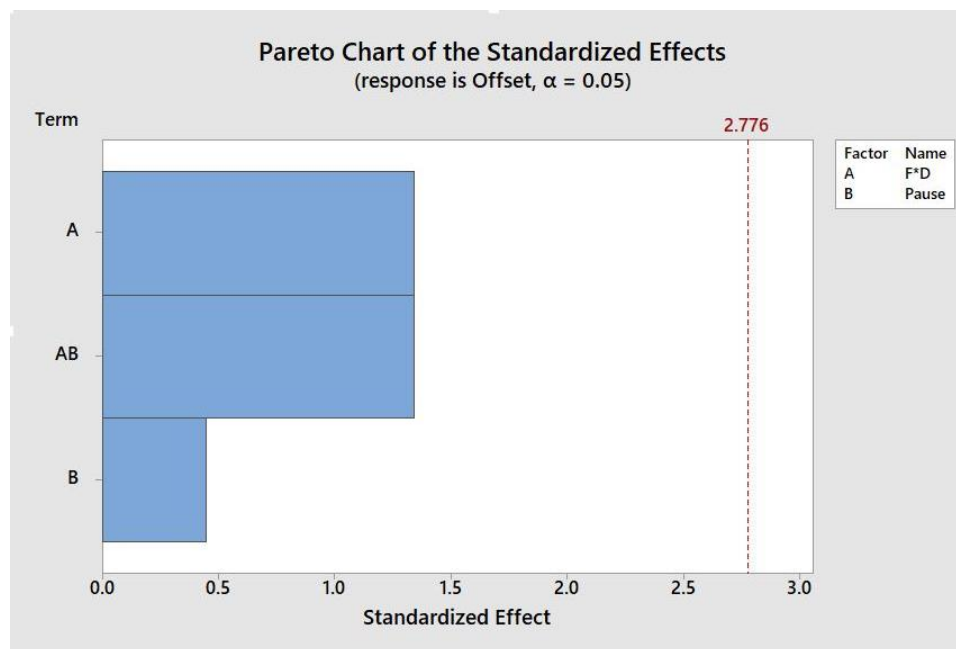


Figure 2: Pareto Chart for DOE of Slice Resolution 1 μm (60 Images)

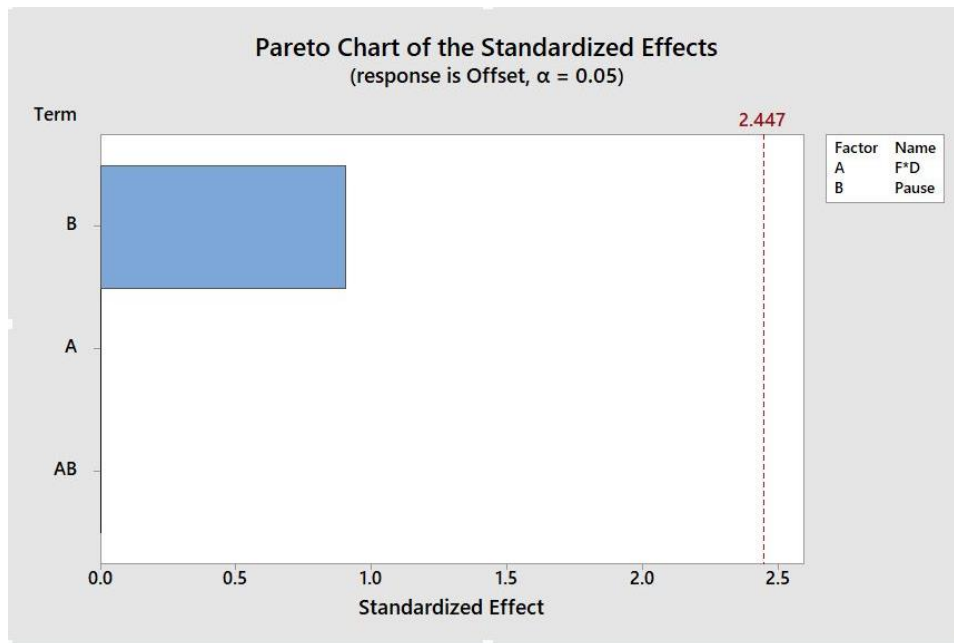


Figure 3: Pareto Chart for DOE of Slice Resolution 0.8 μm (75 Images)

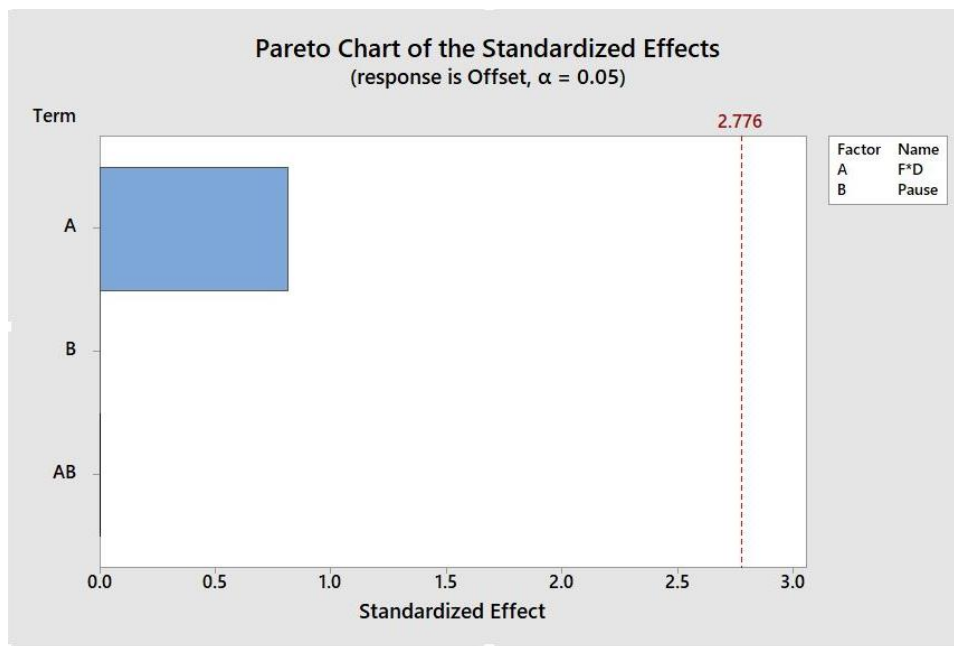


Figure 4: Pareto Chart for DOE of Slice Resolution 0.6 μm (100 Images)

Appendix G: Convergence Testing for Slice Resolution measuring diameter

Figure 1 below shows the convergence data for diameter measurements when investigating an optimal slice resolution value to develop recommendations for the USZ research team. This data supported the decision to recommend 150 images as a conservative estimate to provide representative data outputs for quantitative membrane characterization.

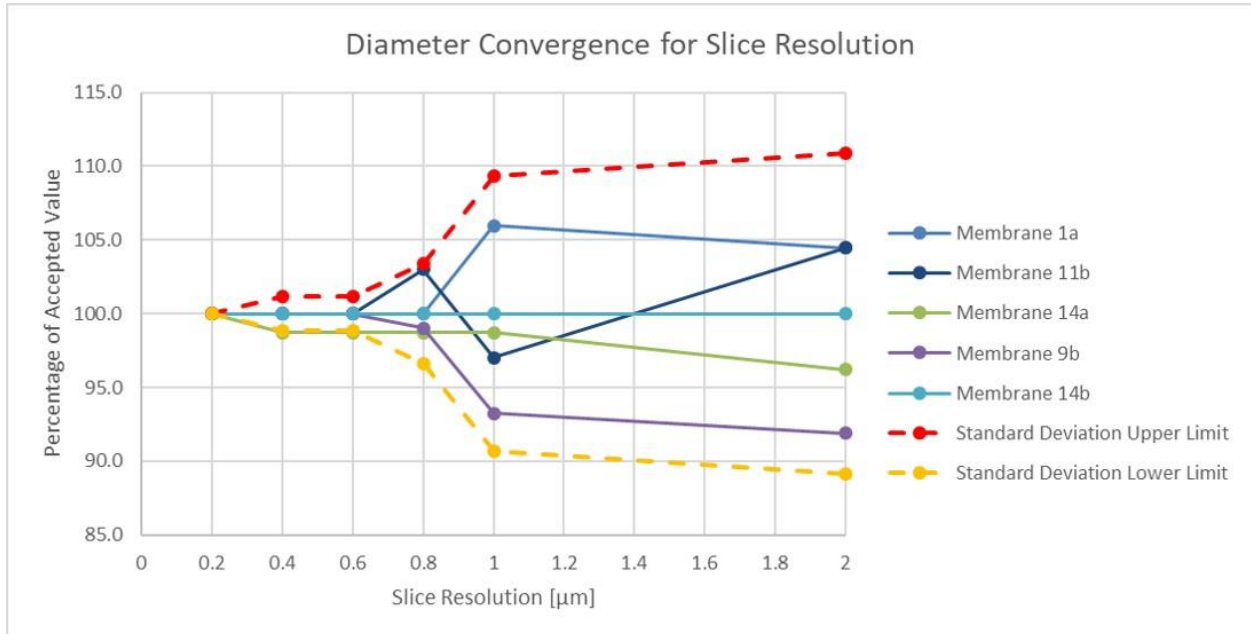


Figure 1: Diameter Convergence for Slice Resolution

Appendix H: Convergence Testing Data Analysis

Convergence testing was completed using a control variable of cell radius to optimize the coarse resolution scale for 150 images. This testing was completed with 4 membranes; 3 membranes with clear curvature and 1 ruptured membrane. This is because these membranes characterize the majority of the population of membranes within each sample holder compared to flat membranes which are uncommon. The four tests for convergence are described in Table 1 below along with the corresponding Figure. The first set of convergence testing for cell radius optimization provided an optimal cell radius of 25 for a coarse resolution scale of 25. To provide a window of optimal cell coarse resolution values, Test 2 (Figures 1 and 2) has a constant cell radius of 20 and Test 3 (Figures 3 and 4) has a constant cell radius of 30.

Table 1: Convergence Testing Data Sets

Measurement	Cell Radius	Cell Pitch Test Values	Convergence Plot
Diameter	30	20, 25, 30, 35, 40	Figure 1
Height	30	20, 25, 30, 35, 40	Figure 2
Diameter	20	20, 25, 30, 35, 40	Figure 3
Height	20	20, 25, 30, 35, 40	Figure 4

Test 2: Convergence Testing for a Cell Radius of 30 pixels

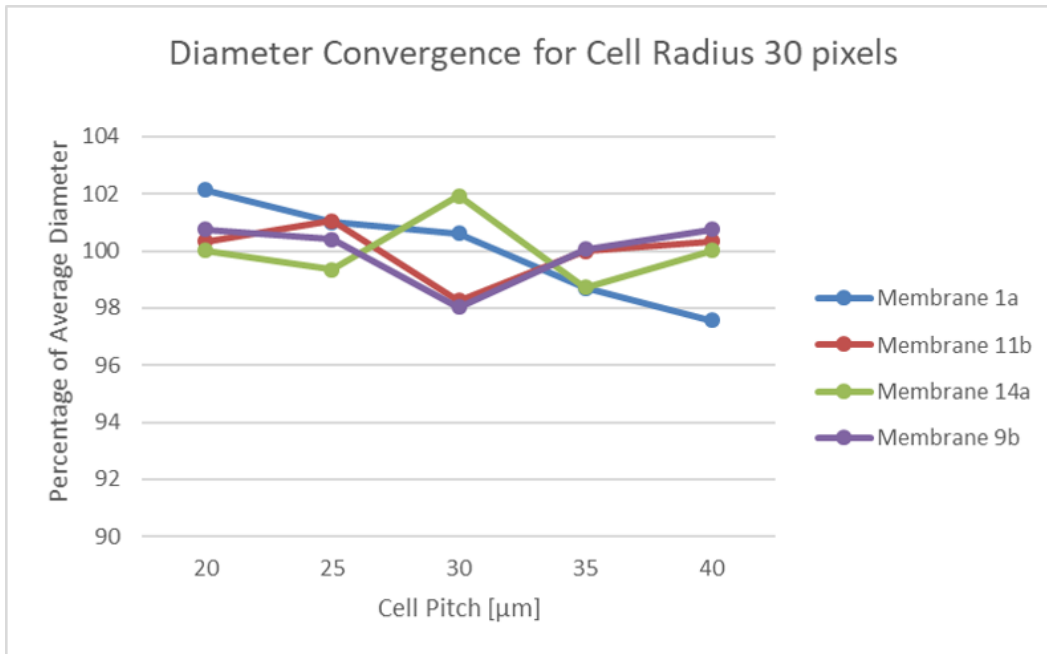


Figure 1: Diameter Convergence plot for a Cell Radius of 30 pixels

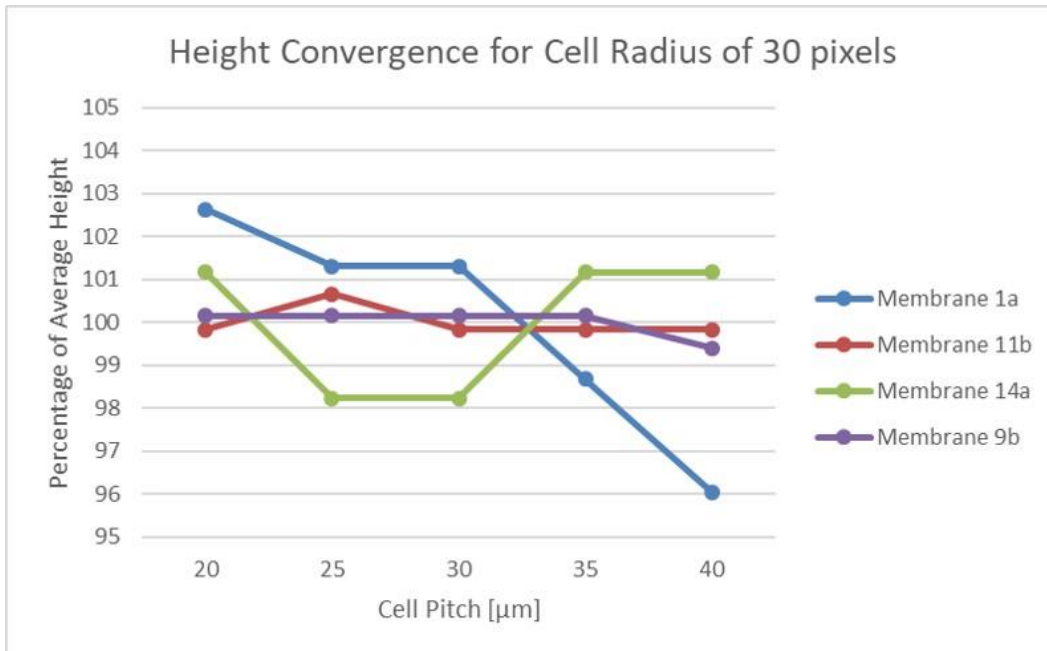


Figure 2: Height Convergence for Cell Radius of 30 pixels

Test 3: Convergence Testing for a Cell Radius of 20 pixels

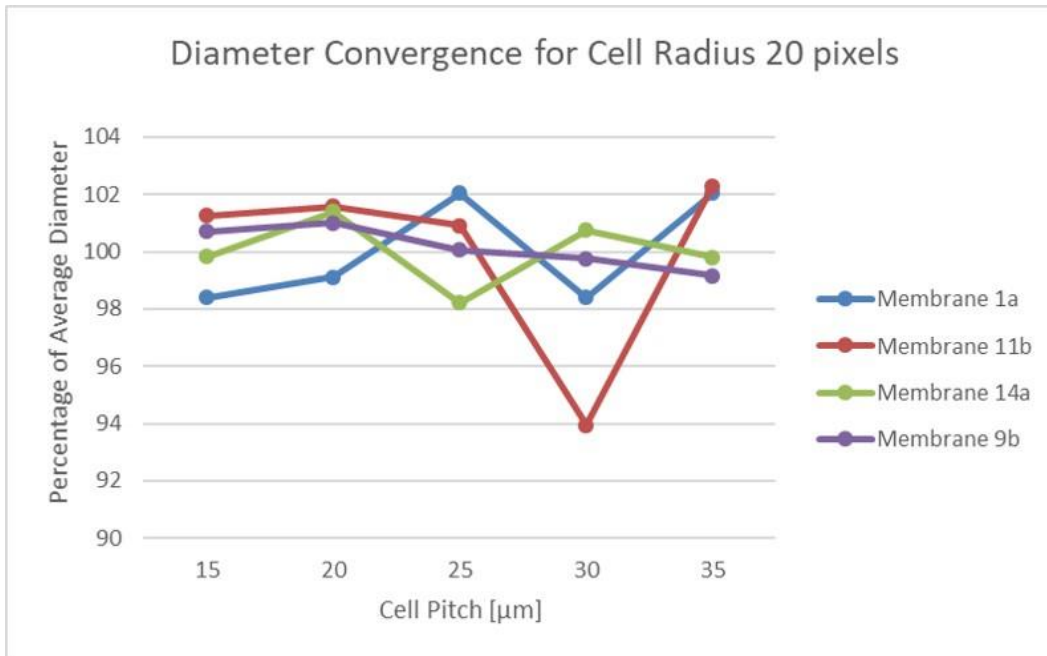


Figure 3: Diameter Convergence Plot with a Cell Radius of 20 pixels

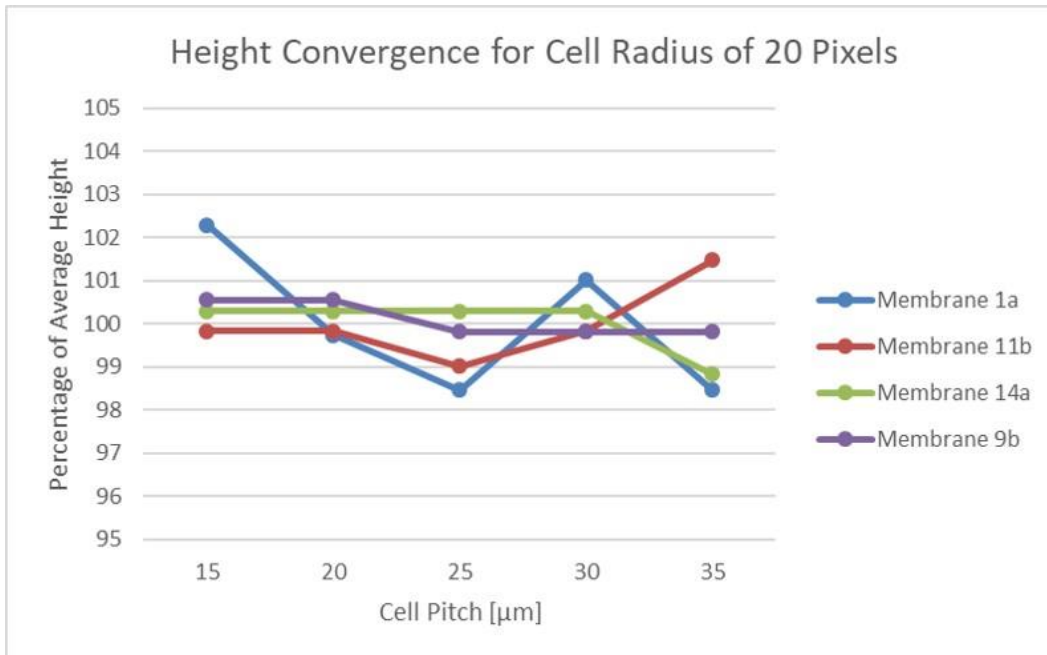


Figure 4: Height Convergence Plot with a Cell Radius of 20 pixels

Appendix I: User Manual for the Automated Leica Microscope Optical Inspection System

Introduction

This manual serves as a guide for usage of the automated optical inspection procedure for Intracochlear Acoustic Receiver (ICAR) hydrophone membranes as of October 11th, 2018. The procedure includes the setup of the automation apparatus, the adjustable parameters for customization of membrane inspection, and expectations for MATLAB output and data collection. All data conclusions are supported through research completed by Worcester Polytechnic Institute (WPI) fourth year students, documented in the report “Automated Optical Inspection of MEMS Based Cochlear Implant Hydrophones”.

Definitions

Membrane: The portion of the ICAR sensor head that registers vibrations.

Sample Holder: The small titanium structure which includes the ICAR sensor heads (Figure 1)

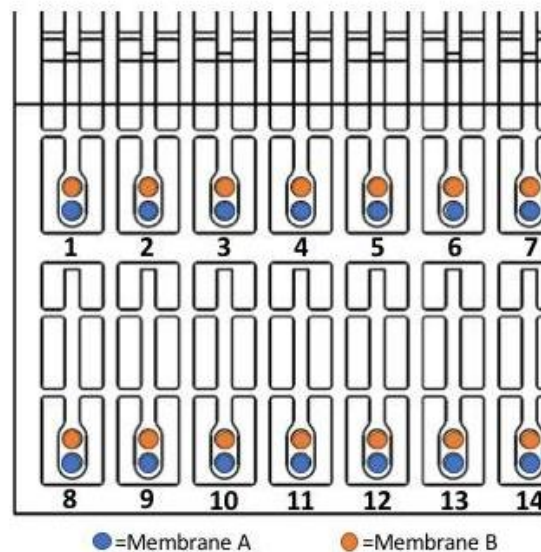


Figure 1: Membrane Sample Holder with suggested naming convention labels

Cell: A group of pixels averaged together (Figure 2).

Cell Radius: The number of pixels from the center of the cell to the cell border (Figure 2).

Cell Pitch: The number of pixels between the center of two cells (Figure 2).

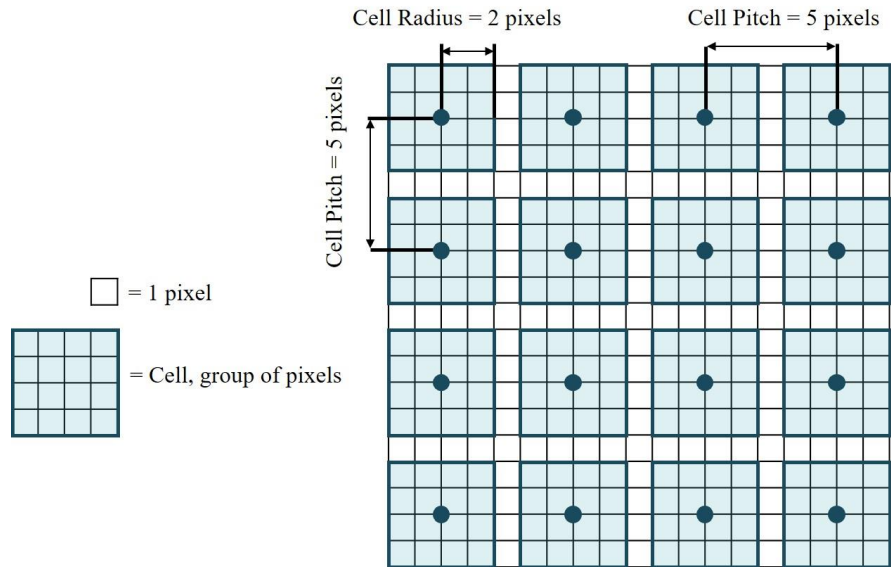


Figure 2: Cell Radius and Cell Pitch Example (scale not representative of actual image size)

Slice Resolution: the specified distance between images for image capture (Figure 3).

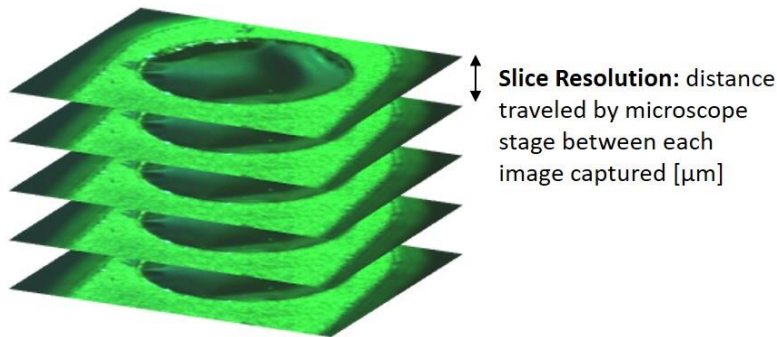


Figure 3: Slice Resolution Example Diagram

MQP_2018_Z_Axis_Image_Capture_Rev3: Script used to automate the Z Axis for incremental movements and image capture

MQP_2018_Image_Processing_Rev1: Revised script used to process images taken with the image capture script

Data_Locations: Directory of file paths where the images are stored from

General Procedure

The procedure outlined in Table 1 includes the automation setup, the image capture process and the post processing procedure for data collection. The expected timing for the complete analysis of 1 membrane with a height of 60 μm and slice resolution of 0.4 μm is conservatively about 45 minutes (15 minutes for setup, 20 minutes for image capture, 5 minutes for post processing, and 5 minutes for diameter and height measurements).

Table 1: Membrane Optical Inspection Procedure with Automated Z-Axis

<ol style="list-style-type: none">1. Experimental Setup<ol style="list-style-type: none">a. Standard Magnification Level: 10x Magnificationb. Standard Microscope Light Setting: “H”c. Plug in AxioCam ICc5 firewire cable to computer prior to opening MATLAB software to ensure the camera is recognized.d. Attach the Z-Axis dial adapter to the Z-Axis fine focus dial. Align stepper motor platform with the focusing dial and position motor to keep the belt centered and taught.e. Plug the USB printer cable into the Arduino port and the computer USB port for motor control.f. Disengage the Emergency Stop button and switch the power supply to the “Off” position. Plug the 15V power supply into a wall outlet.
<ol style="list-style-type: none">2. Software Setup<ol style="list-style-type: none">a. Open the “MQP_2018_Z_Axis_Image_Capture_Rev3” MATLAB image capture script.b. Prior to running the script, define the folder path for the saved images in the “Setup Variables” module for the “image_path” variable. If you do not change the folder destination for each membrane, the images will write over each other.c. Ensure Z-axis stepper motor digital pin connections (ex: D07) correspond to the MATLAB variables for “axis_1_step_pin” and “axis_1_dir_pin” which define the pins step and direction pins respectively.
<ol style="list-style-type: none">3. Center Membrane for Image Capture<ol style="list-style-type: none">a. Open the MATLAB Image Acquisition toolbox and choose the “F7_RGB24_2452x2056_mode0” camera setting.<ol style="list-style-type: none">i. Note: If the camera connection does not appear, close MATLAB, then disconnect and reconnect the camera, and re-open MATLAB.b. Click “Start Preview” to view the membrane through the AxioCam ICc5 on the computer screen.<ol style="list-style-type: none">i. Note: The image shown in the MATLAB preview will look different from the view seen through the microscope lens.c. Check that the light filter is completely open for correct image capture lighting.

4. Focus on Titanium Surface

- a. Focus on the top titanium surface of the hydrophone sensor structure using the Z-Axis dial (Figure 4).
 - i. Note: If the switch on the emergency stop button is set to the “On” position, the Z-Axis dial cannot be moved manually.
 - ii. Note: The MATLAB image capture script will move 2 μm up from the focused surface to account for user error

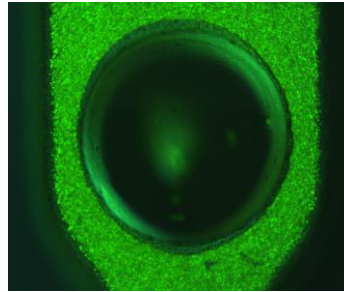


Figure 4: Example of top titanium surface in focus

5. Turn on Power Supply

- a. Move the switch for the battery supply to the “On” position. The stepper motor will produce a low humming noise when connected to the battery and the Z-Axis dial can no longer be turned manually.

6. Run Image Capture MATLAB Script

- a. Press “Run” within the MATLAB window
- b. Define the following parameters in the pop-up windows:
 - i. Preferred Image Name: enter a base name for the image files, for example “Test_Image”
 - ii. Total Height: enter the total height to capture images in microns, for example 60 μm
 - iii. Slice Resolution: enter the slice resolution, distance between each image in microns, as a number from the options available in Table 2
 - iv. Image Capture Settings: enter as either “RGB” or “RAW” for color or grayscale image capture
- c. After the parameters have been setup, the stepper motor will move and images will be captured and saved to the specified folder path.

Note: The total number of images captured is equivalent to the total height divided by slice resolution, rounded to the nearest whole number. Image capture and processing time will increase as the number of images captured increases.

Transition to Image Processing for Membrane Modelling

7. Image Processing MATLAB Script

- a. Open “MQP_2018_Image_Processing_Rev1” and press “Run”
- b. Define the following parameters in the pop-up windows:
 - i. Data Index: enter the proper data index value corresponding to the index defined in the “Data_locations” MATLAB script
 - ii. Image Base Name: enter the same image base name used for Image Capture, for example “Test_Image”
 - iii. Slice Resolution: enter the same slice resolution value used in the image capture process

8. Completion of Script

- a. The “MQP_2018_Image_Processing_Rev1” script will output a 2D plot and 3D model. The 3D model represents the complete membrane shape and the 2D plot represents the average cross-sectional shape for measurements.

9. Measure Diameter and Height

- a. In the 2D plot open the Data Cursor, found under the “Tools” menu
- b. Define three characteristic points on the black averaged depth line (Figure 5).
 - i. Note: To create a new data point “Shift+Click” or right click “Create New Data Tip”
- c. Use the three characteristic points to calculate the height and diameter.

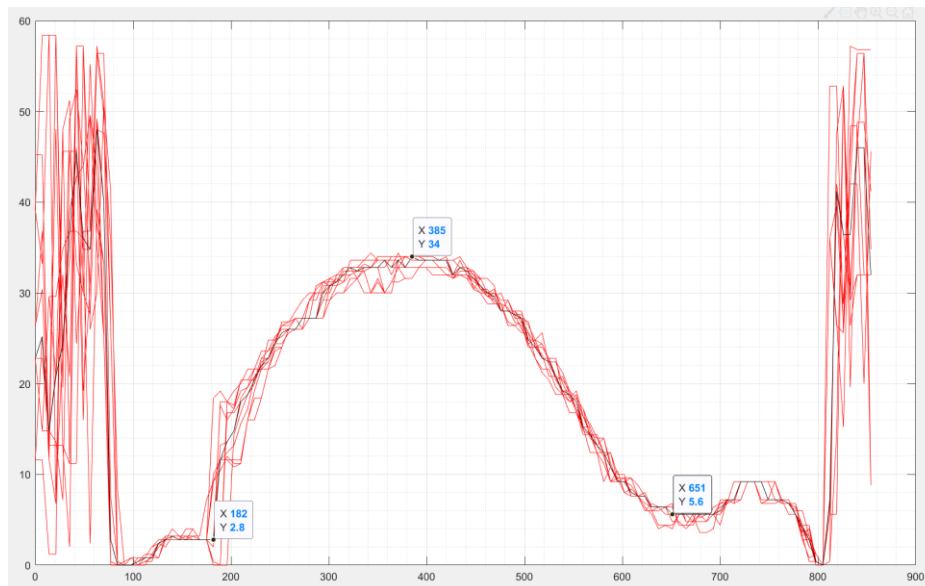


Figure 5: Example 2D plot output and data points for height and diameter measurements

Customizable Settings

Note: All WPI Team recommendations are based on research and testing described in the report “Automated Optical Inspection of MEMS Based Cochlear Implant Hydrophones”

Image Capture: Slice Resolution

All values are based on 60 μm image capture height span. Changing the “slice_res” in the MATLAB script will affect the amount of interpolation between data points. Increasing the slice resolution (decreasing the number of images) will make the 3D shape plot appear rough. Decreasing the slice resolution (increasing the number of images) will make the 3D plot appear smooth as there is more data to represent membrane shape.

Note: The WPI Team recommends a “slice_res” value of 0.4 μm (150 images over 60 μm).

Table 2: Available settings for incremental stepping during image capture

No. of Images	μm Traveled per image (slice_res)	\pm Tolerance Diameter	\pm Tolerance Height	Average Time for Image Processing
30	2	10.9%	7.0%	2.4 min
60	1	9.3%	7.1%	4.1 min
75	0.8	3.4%	5.1%	5.3 min
100	0.6	1.1%	2.7%	6.7 min
150	0.4	1.1%	2.4%	10.4 min
300	0.2	0%	0%	21.8 min

Image Capture: RGB and RAW

Changing the settings for image capture from the values below will alter the appearance of the image. This may affect the focus calculations for data collected using the new settings. These settings can be accessed through the “RGB_Camera_Settings” and “RAW_Camera_Settings” MATLAB scripts.

Note: The WPI Team recommends using the values listed in the table below.

Table 3: Available settings for image capture

RGB	RAW
src.Brightness = 684; src.BusSpeed = 'S200'; src.BytesPerPacket = 2048; src.Exposure = 235; src.Gain = 116; src.Shutter = 4095; src.Hue = 128; src.Sharpness = 2;	src.Brightness = 0; src.BusSpeed = 'S200'; src.BytesPerPacket = 2048; src.Exposure = 235; src.Gain = 0; src.Shutter = 4095; src.Hue = 256; src.Sharpness = 4;

Image processing: Cell Radius/Cell Pitch

Changing cell radius and cell pitch values will alter how the focus of each image is calculated. The lower values create a more fine focusing calculation versus the higher values which create a coarser focusing calculation. If the focusing calculation is too fine, the data output may show more noise than expected. If the focusing calculation is too coarse, the data output may not be representative of the membrane shape.

Note: The WPI Team recommends using a cell radius of 25 pixels and a cell pitch of 25 pixels. This combination requires 5 minutes of processing time for 150 images.

Table 4: Optimal Cell Radius and Cell Pitch Scale Parameters for MATLAB Script Variables

Cell Radius (pixels)	Cell Pitch (pixels)	Average Processing Time with 150 images [min]
30	30, 35	5.25, 3.9
25	25	5
20	20	5.5